HHS Public Access

Author manuscript

Neuron. Author manuscript; available in PMC 2018 February 22.

Published in final edited form as:

Neuron. 2017 February 22; 93(4): 867–881.e6. doi:10.1016/j.neuron.2017.01.010.

Axonal endoplasmic reticulum Ca^{2+} content controls release probability in CNS nerve terminals

Jaime de Juan-Sanz[1], **Graham T. Holt**[2], **Eric R. Schreiter**[2], **Fernando de Juan**[3], **Douglas S. Kim**[2], and **Timothy A. Ryan**[1,*]

[1]Department of Biochemistry, Weill Cornell Medicine, New York, New York 10065, USA

[2]Janelia Research Campus, Howard Hughes Medical Institute, Ashburn, Virginia 20147, USA

[3]Department of Physics, University of Oxford, Oxford OX1 3NP, United Kingdom

Abstract

Although the endoplasmic reticulum (ER) extends throughout axons and axonal ER dysfunction is implicated in numerous neurological diseases, its role at nerve terminals is poorly understood. We developed novel genetically-encoded ER-targeted lowaffinity Ca^{2+} indicators optimized for examining axonal ER Ca^{2+}. Our experiments revealed that presynaptic function is tightly controlled by ER Ca^{2+} content. We found that neuronal activity drives net Ca^{2+} uptake into presynaptic ER although this activity does not contribute significantly to shaping cytosolic Ca^{2+} except during prolonged repetitive firing. In contrast we found that axonal ER acts as an actuator of plasma membrane (PM) function: $[Ca^{2+}]_{ER}$ controls STIM1 activation in presynaptic terminals, which results in the local modulation of presynaptic function, impacting activity-driven Ca^{2+} entry and release probability. These experiments reveal a critical role of presynaptic ER in the control of neurotransmitter release and will help frame future investigations into the molecular basis of ER-driven neuronal disease states.

INTRODUCTION

Although the existence of axonal ER has been well documented (Henkart et al., 1978; Tsukita and Ishikawa, 1976), how presynaptic ER dysfunction impacts synaptic function is poorly understood, making it difficult to understand how genetic lesions in ER proteins contribute to neurological disease states. For example, several axonopathies arise from mutations in ER proteins: genetic lesions in reticulon-2, REEP1 and atlastin-1 lead to hereditary spastic paraplegia, while mutations in VAP-B are causative agents in amyotrophic lateral sclerosis (Blackstone et al., 2011; Montenegro et al., 2012; Noreau et al., 2014;

*correspondence & lead contact: taryan@med.cornell.edu.

AUTHOR CONTRIBUTIONS

Experiments were designed by J.J-S. and T.A.R. F.J. developed the quantitative procedures to estimate $[Ca^{2+}]_{ER}$. G.T.H. and E.R.S. characterized *in vitro* properties of purified low affinity GCaMPs under the supervision of D.S.K. All other experiments were carried out by J.J-S. The manuscript was written by J.J-S. and T.A.R.

Teuling et al., 2007). Additionally, alterations of ryanodine receptor 2 are linked to cognitive dysfunction (Liu et al., 2012) and studies of the genetic loss of the γ-secretase complex strongly imply that certain penetrant mutations in familial Alzheimer's disease alter ER Ca^{2+} handling at nerve terminals (Zhang et al., 2009). One well-known function of the smooth ER is its role as a Ca^{2+} handling organelle but there is little understanding of how perturbations in this process impact synaptic function (Verkhratsky, 2005). In general, ER Ca^{2+} store function can be separated into 2 roles: first, it can influence biochemical events by acting as a local source or sink of Ca^{2+}. Second, the ER can act as an actuator of plasma membrane (PM) function at ER-PM contacts, a function controlled by the Ca^{2+} concentration within the ER lumen ($[Ca^{2+}]_{ER}$). The best-established example of this second role is the activation of Orai, a PM-Ca^{2+} channel, by stromal interaction molecule 1 (STIM1), an ER-Ca^{2+} sensor (Hogan and Rao, 2015; Liou et al., 2005; Zhang et al., 2005), although a number of other PM targets of STIM1 have been identified (Hooper et al., 2013). One challenge in determining which role is operational is the absence of sufficiently sensitive tools to directly monitor $[Ca^{2+}]_{ER}$ during genetic, physiological or pharmacological ER manipulations. This is particularly challenging in small compartments like axons, where the ER occupies an even smaller volume. In general, previous approaches aimed at understanding the role of axonal Ca^{2+} stores monitored only cytosolic Ca^{2+} during ER manipulations, not $[Ca^{2+}]_{ER}$ itself. To circumvent this problem and gain insight into how ER Ca^{2+} contributes to synaptic transmission we designed and optimized genetically-encoded ER-targeted Ca^{2+} sensors based on GCaMP, selected such that the affinity was lowered to match resting axonal $[Ca^{2+}]_{ER}$ but maintaining high responsiveness upon binding to Ca^{2+}. These new tools (ER-GCaMP6-150, ER-GCaMP6-210) allowed robust measures of Ca^{2+} dynamics in axonal ER during electrical activity for the first time and provided a precise approach to determine the consequences of pharmacological and genetic manipulations of ER function. These experiments demonstrated that resting $[Ca^{2+}]_{ER}$ levels are on average ~150 μM but vary from cell to cell. This variation is correlated with presynaptic function, but this correlation depends on STIM1. Furthermore, pharmacological perturbations that lower $[Ca^{2+}]_{ER}$ and inhibit presynaptic Ca^{2+} influx and exocytosis also depend on STIM1 and its ability to sense Ca^{2+} via his luminal EF hand domain. Thus, ER Ca^{2+} content is a critical control parameter for neurotransmitter release and maintenance of ER health is essential for proper control of synaptic function.

RESULTS

Maintenance of axonal ER Ca^{2+} handling is critical for presynaptic function at physiological temperature

To examine ER's role in synaptic transmission and the behavior of ER Ca^{2+} during activity we used primary dissociated hippocampal neurons as they allow using robust quantitative optical tools to dissect molecular function (Hoppa et al., 2012; Rangaraju et al., 2014). We examined how blocking the major ER Ca^{2+} influx pathway mediated by sarco/endoplasmic reticulum Ca^{2+}-ATPases (SERCAs) impacts both presynaptic Ca^{2+} signals and exocytosis at nerve terminals in response to single action potential (AP) firing at 37°C. Single AP-driven cytosolic Ca^{2+} signals arising from voltage-gated calcium channel (VGCC) opening at synaptic boutons were measured using Fluo-5F AM in regions identified with the

presynaptic marker VAMP–mCherry (Calloway et al., 2015; Hoppa et al., 2012) whereas synaptic vesicle exocytosis was measured using the optical reporter vGlut1–pHluorin (vG-pH) (Ariel et al., 2012; Armbruster and Ryan, 2011). We found that application of the potent SERCA inhibitor cyclopiazonic acid (CPA, 50 μM) led to a significant reduction in both single-AP-driven Ca^{2+} signals (Fig. 1A) and exocytosis (Fig. 1B). Identical results were obtained using a genetically encoded Ca^{2+} indicator, GCaMP6f (Fig. S1A), as well as with an alternative SERCA blocker, Thapsigargin (TG, 1 μM) (Fig. S1B-C), making it unlikely that the reduction in Ca^{2+} signals is arising from an off-target effect. SERCA blockade led to a small increase in baseline fluorescence in dendrites without a significant impact in axons (see methods and Fig. S1D, E). Although such reduction in presynaptic Ca^{2+} signals during SERCA blockade has previously been reported in a number of synaptic preparations (Emptage et al., 2001; Liang et al., 2002), others concluded that similar manipulations of ER Ca^{2+} handling had little impact on presynaptic function (Beck et al., 2001; Carter et al., 2002). We noticed a striking correlation in the published literature regarding this issue: experiments performed at temperatures significantly colder (room temperature 22–26°C) than what would be physiological (37°C) for a rodent preparation observed that SERCA blockage had little impact on presynaptic function whereas experiments performed at 30–32°C found a reduction in activity-driven Ca^{2+} signals. We repeated our measurements at a cooler temperature (26°C) and found that CPA had little impact on either AP-driven presynaptic Ca^{2+} entry (Fig. 1C, E) or exocytosis (Fig. 1D, F). Thus, the experimental temperature is critical for revealing the importance of ER Ca^{2+} handling in synaptic function and these experiments provide a plausible explanation for previous results that came to contradictory conclusions (Beck et al., 2001; Carter et al., 2002). The simplest interpretation of our results implies that the ER normally acts as a net source of Ca^{2+} during an AP, perhaps via calcium-induced Ca^{2+} release (CICR). However, the normally tight coupling of Ca^{2+} entry and exocytosis dictates that exocytosis is dominated by Ca^{2+} entry in the active zone restricted to domains near voltage-gated Ca^{2+} channels (Llinas et al., 1992; Stanley, 1997) and would unlikely be influenced by more distant sources of Ca^{2+} such as those from internal stores. In order to understand how ER Ca^{2+} handling could be impacting presynaptic function we sought to directly examine ER Ca^{2+} dynamics.

A new generation of ultrasensitive ER Ca^{2+} indicators

Understanding the biology of ER Ca^{2+} fluxes in axons and nerve terminals is currently constrained by the paucity of techniques suitable for detecting ER Ca^{2+} dynamics that arise in such small volumes. To solve this problem we took advantage of a previous screening effort for generating novel genetically encoded calcium indicators (Chen et al., 2013) and focused on newly-generated GCaMP variants that *in vitro* presented Ca^{2+} binding affinities reduced by a factor of ~500–1000 but maintained high responsiveness upon binding to Ca^{2+} (i.e. high dynamic range). We selected 4 variants with different affinities to study further, which were divided in two classes depending on their responsiveness: GCaMP3 (dynamic range: 13–14) and GCaMP6 (dynamic range: 45–48). Each variant's name ends with a number that indicates its K_d for Ca^{2+} in μM. The variants used in this study are: GCaMP3-44, GCaMP6-150, GCaMP6-210 and GCaMP3-373 (Fig. 2A; Table 1). Note that GCaMP3-373 is a variant previously published as GCaMPer-10.19 (Henderson et al., 2015) but renamed here to maintain a comprehensive nomenclature. These variants were expressed

in excitatory primary neurons under the CaMKII promoter and were specifically targeted to the ER using a well-established approach that is based on adding the N-terminal signal peptide of calreticulin and the C-terminal KDEL retention motif (Kendall et al., 1994; Kiyonaka et al., 2013; Miyawaki et al., 1997; Munro and Pelham, 1987) (see methods). High-resolution confocal imaging in cell somas expressing ER-targeted GCaMP6-150 (ER-GCaMP6-150) showed a detailed reticular network in the cell soma (Fig. 2B) that extended throughout dendrites and the entire length of the axon including presynaptic boutons (Fig. 2C).

Estimates of the resting Ca^{2+} concentration in neuronal ER

In order to estimate $[Ca^{2+}]_{ER}$ in hippocampal excitatory neurons we developed a protocol that relies on measuring the change in fluorescence during indicator saturation by application of the Ca^{2+} ionophore ionomycin (see methods), which rapidly saturates ER-GCaMPs signals after 1–2 min of treatment (Fig. 2D). To obtain a robust estimate of $[Ca^{2+}]_{ER}$ we applied this protocol to neurons separately expressing each of our four selected ER-GCaMP variants and measured somatic fluorescence changes. We found higher saturation peak values for the indicators with lower affinities (Fig. 2E). Combined with the measured *in vitro* properties of the different indicators (Table S1), the fluorescence increase during ionomycin application allowed us to estimate the pre-ionomycin $[Ca^{2+}]_{ER}$ value (see methods). All four ER-GCaMP variants tested led to very similar estimates of resting $[Ca^{2+}]_{ER}$, ranging from 135 to 165 μM (average of the four estimates 152 ± 8 μM) (Fig. 2F). These estimates were additionally corrected for the small change in ER pH induced by ionomycin (Fig. S2A, see methods) that affects the fluorescence of each indicator differently depending on their pKa in the Ca^{2+} bound state (Table S1).

Action potential firing drives a net Ca^{2+} uptake into the ER

To compare the ability of each indicator to detect physiological ER Ca^{2+} dynamics during AP firing we used ER-GCaMPs and the previously published ER Ca^{2+} indicator G-CEPIA1er (Suzuki et al., 2014) to measure somatic ER Ca^{2+} handling during a brief burst of activity (20AP at 20Hz). In general, the net behavior of ER Ca^{2+} during activity will depend on the relative abundance of Ca^{2+} uptake mechanisms, such as those mediated by SERCAs, and ER Ca^{2+} efflux pathways, for example mediated by IP_3 receptors and ryanodine receptors (Foskett et al., 2007; Liu et al., 2012), and the extent to which each of these are activated during a given stimulus. For the stimulus used here, a 1 second 20 AP burst, all indicators reported an increase in fluorescence indicating a net active uptake of calcium into somatic ER (Fig. 3A-C). The largest signals were obtained using ER-GCaMP6-150 and ER-GCaMP6-210 sensors, likely due to the better dynamic range and proximity of the affinities to resting $[Ca^{2+}]_{ER}$ of these probes (Fig. 2A, table S1). We verified that this level of activity does not impact ER pH in somas using an ER targeted pHluorin (data not shown). In addition, we failed to detect any signal from these low affinity Ca^{2+} indicators when expressed in the cytosol (for which the ER-targeting sequences were removed) (see below), indicating that these ER Ca^{2+} signals were not contaminated by any possible miss-targeted ER-GCaMPs in the cytosol.

We next examined both resting ER Ca^{2+} and activity-driven dynamics in nerve terminals in response to AP firing. Using the same procedures above we measured $[Ca^{2+}]_{ER}$ in axons using ER-GCaMP-150, of which the affinity for Ca^{2+} is best matched to the likely resting value (Table S1). These experiments showed that somatic and axonal $[Ca^{2+}]_{ER}$ values are not significantly different, as expected from the continuity of the organelle through the neuron (somatic $[Ca^{2+}]_{ER}$ = 164 ± 7 μM, n = 8; axonal $[Ca^{2+}]_{ER}$ = 156 ± 15 μM, n = 15, n.s. p=0.78). Whether the ER at nerve terminals acts as a net source or sink for cytoplasmic Ca^{2+} during activity has been a subject of debate (Verkhratsky, 2005). We co-transfected hippocampal neurons with plasmids encoding each ER-GCaMP variant and VAMP-mCherry (Fig. 2D, E), which allows easy identification of nerve terminals. ER-GCaMP3 variants and G-CEPIA1er failed to reveal any signal during activity in nerve terminals (data not shown) whereas both ER-GCaMP6-150 and ER-GCaMP6-210 presented robust signals. Since resting $[Ca^{2+}]_{ER}$ is estimated to be ~150 μM we carried out the majority of our subsequent experiments using ER-GCaMP6-150. These experiments showed that, similar to what was observed in somas, axonal ER acts a buffer for Ca^{2+}, rapidly taking up Ca^{2+} during AP firing (Fig. 3D–F; $\Delta F/F_0$ (20AP) = 0.53 ± 0.04, n=64). Activity-driven increase in $[Ca^{2+}]_{ER}$ returned to baseline levels following a single exponential decay with an average decay constant of τ=8.1 ± 0.7 s. These experiments demonstrate that presynaptic ER acts as a net but transient sink during Ca^{2+} elevations driven by electrical activity. Single AP stimulation also resulted in net ER Ca^{2+} uptake (see below). These signals are ER-specific since GCaMP6-150 expressed in the cytosol was not able to detect any response (cyto-GCaMP6-150, Fig. 3F) and were not corrupted by potential changes in ER pH as ER-pHluorin reported no pH changes in axonal ER during such brief bursts of stimulation (Fig. S2B). Using our ionomycin-based estimate of the average resting $[Ca^{2+}]_{ER}$, the measured change in ER-GCaMP6-150 fluorescence ($\Delta F/F_0$) in response to 20 AP stimuli corresponds to an average transient increase in axonal $[Ca^{2+}]_{ER}$ of $\Delta[Ca^{2+}]_{ER}$=122 ± 11 μM S.E.M. (n=64).

It is also possible to derive estimates of both resting $[Ca^{2+}]_{ER}$ and the change in $[Ca^{2+}]_{ER}$ during activity in somas and axons by comparing pair-wise the average magnitude of the activity-driven increases in fluorescence obtained from probes with different affinities for Ca^{2+} (see methods). This approach does not make any assumptions about the ability of ionomycin to saturate the probes in the ER and relies only on using the measured *in vitro* properties of the different indicators and how these indicators respond to a given stimulus. Data obtained using this additional approach are summarized in figure S3 and in general reveal broad agreement for the ionomycin and activity-based estimates. Our data thus strongly support the idea that at nerve terminals during brief AP firing the ER acts as net local sink for Ca^{2+}, not as a net local source.

Activity-driven Ca^{2+} uptake into axonal ER depends on SERCAs

In many cell types constitutive refilling of intracellular Ca^{2+} stores is pivotal for maintaining intracellular Ca^{2+} homeostasis and it is mediated by SERCAs. We verified that presynaptic ER Ca^{2+} uptake is mediated by SERCAs by examining the impact of pharmacological blockade of SERCAs on AP-driven ER Ca^{2+} signals. These experiments demonstrated that activity-driven transient increases in axonal $[Ca^{2+}]_{ER}$ driven by 20 AP (Fig. 4A) or even one

AP (Fig. 4B) were eliminated by application of CPA. Single AP ER Ca^{2+} signals were measured using ER-GCaMP6-210, which provided a slightly better signal to noise ratio than ER-GCaMP6-150 in this regime. Furthermore, these data indicate that ER Ca^{2+} uptake appears to scale roughly linearly with stimulus number (single AP $\Delta[Ca^{2+}]_{ER}$ ~ 6 μM, 20 AP $\Delta[Ca^{2+}]_{ER}$ ~ 120 μM). Complete inhibition of ER Ca^{2+} uptake was also observed with the two other commonly used SERCA inhibitors, thapsigargin (TG, 1 μM) and 1,4-dihydroxy-2,5-di-tert-butylbenzene (BHQ, 50 μM) (Fig. 4C). These results demonstrate that the transient uptake of Ca^{2+} into the ER during action potential firing requires SERCA function and suggest that the assumption that there is net release of Ca^{2+} from the ER at nerve terminals during AP firing is incorrect.

Presynaptic inhibition is slower than ER Ca^{2+} depletion following SERCA block

The fact that blocking ER Ca^{2+} handling inhibits cytosolic Ca^{2+} signals and exocytosis (Fig. 1) even though the ER is not acting as a net source of Ca^{2+} in axons (Fig. 4) implies that a more complex mechanism is linking presynaptic function at the plasma membrane to ER Ca^{2+} handling. To better understand the mechanism by which SERCA blockade modulates presynaptic plasma membrane function we compared the time course of presynaptic $[Ca^{2+}]_{ER}$ and the time evolution of AP-triggered peak cytosolic Ca^{2+} during application of CPA. In neurons and other cell types SERCA pump activity continuously counteracts Ca^{2+} leakage from the ER to the cytosol, resulting in balanced uptake/leak fluxes that maintain constant $[Ca^{2+}]_{ER}$ levels (Verkhratsky, 2005). Blocking ER Ca^{2+} uptake leads to $[Ca^{2+}]_{ER}$ depletion, a cellular dysregulation that is associated with many neurological disorders (Mekahli et al., 2011). We found that CPA application led to a depletion of axonal $[Ca^{2+}]_{ER}$ over a <1 min time scale both at 26°C ($\tau_{\text{ ER depletion}}$=47.5 ± 3.5 s) and 37°C ($\tau_{\text{ ER depletion}}$=26.0 ± 0.9 s), with $[Ca^{2+}]_{ER}$ stabilizing to a new level of ~100 μM in both cases ($\Delta[Ca^{2+}]_{ER}$(26°C)= −39 ± 3 μM, $\Delta[Ca^{2+}]_{ER}$(37°C)= −48 ± 6 μM), at which point any further activity-driven ER Ca^{2+} signals were eliminated (Fig. 5A, B). The block of ER Ca^{2+} uptake had little impact on presynaptic single AP-driven Ca^{2+} signals at 26°C (Fig. 5D, G) while at 37°C the reduction of cytosolic Ca^{2+} signals occurred at a 5–6 fold slower rate than the corresponding $[Ca^{2+}]_{ER}$ depletion (Fig. 5E, H; $\tau_{\text{ cyto Ca }^{2+}}$= 148 ± 18 s). The fact that modulation of presynaptic function is much slower than $[Ca^{2+}]_{ER}$ depletion implies that inhibition in exocytosis and AP-evoked Ca^{2+} signals are not simply due to loss of either an ER Ca^{2+} uptake or efflux pathway. Instead, it suggests that changing ER Ca^{2+} drives a slower control mechanism that is manifest at the plasma membrane. The absence of any impact on single AP-driven changes in Ca^{2+} after SERCA inhibition at 26 °C (Fig. 1C, Fig. 5D) also implies that the absolute ER Ca^{2+} fluxes at nerve terminals are likely small compared to single AP-triggered VGCC-mediated cytosolic Ca^{2+} entry and extrusion. In fact, block of ER Ca^{2+} uptake at 26°C only impacted Ca^{2+} accumulation during prolonged stimulus trains, leading to a modest increase in cytosolic Ca^{2+} discernable after 60AP or more (n=8, *p<0.05; Fig. S4A) and an increase in exocytosis observable only after 100 AP stimuli (n=7, *p=0.03; not shown). Together these data all provide strong evidence that although presynaptic ER can rapidly sequester cytosolic Ca^{2+} during activity, the direct impact on shaping cytosolic Ca^{2+} dynamics is relatively minor. Instead our data reveal an unexpected feedback loop whereby the content of the ER drives a change in plasma

membrane function (Fig. 5) that is not apparent at a temperature only 11°C below the physiological temperature over a 10 min time period (Fig. 5G).

Presynaptic function correlates with ER Ca^{2+} content

The fact that reduced ER Ca^{2+} content results in the inhibition of Ca^{2+} influx and exocytosis at the plasma membrane (Fig. 5) suggests that $[Ca^{2+}]_{ER}$ might be a key control parameter for presynaptic function. To test this idea, we measured axonal $[Ca^{2+}]_{ER}$ in individual neurons at 37 °C and measured the corresponding presynaptic single AP-evoked Ca^{2+} cytosolic signals in the same axons using the red Ca^{2+} indicator jRCaMP1b, which required increasing external Ca^{2+} up to 4mM to improve signal-to-noise (Dana et al., 2016). Single AP stimulation resulted an average ΔF/F change of 0.09 ± 0.01, similar to previously reported (Dana et al., 2016), and its expression did not affect ER Ca^{2+} content (axonal $[Ca^{2+}]_{ER}$ when expressing jRCaMP1b = 169 ± 8 μM, n.s. p = 0.43 compared to control). Remarkably, these experiments revealed a significant correlation between ER Ca^{2+} content and presynaptic Ca^{2+} entry on a cell-by-cell basis (Spearman's correlation coefficient ρ=0.6; * p=0.02) (Fig S6A; see methods). To reduce observational noise found in the raw data (presented in Fig. S6A) we binned these data, which allows obtaining a better estimate of the parameters in the fitting (Fig. 6A; see methods). The correlation observed shows a saturable relationship and appears reasonably well described by a generalized Hill equation (see methods), with a Hill coefficient n=5.4 and an apparent have maximal activation constant ($K_{1/2}$ ~105μM). The average drop in $[Ca^{2+}]_{ER}$ resulting from SERCA block (~50 μM) also predicts a concurrent drop in Ca^{2+} influx of ~45%, similar to what we observe experimentally (~35%; Fig. 5F). These data support the idea that the natural variation in ER Ca^{2+} content across cells is a potential driver of synapse function via a feedback loop connecting ER Ca^{2+} and plasma membrane function. To test the veracity of this idea we sought to determine 1) the key molecular driver of the feedback loop and 2) to examine both the correlation between ER Ca^{2+} and plasma membrane function and the impact of ER Ca^{2+} depletion when the feedback loop is disabled.

Loss of STIM1 disables the feedback loop linking ER Ca^{2+} content to presynaptic Ca^{2+} influx and exocytosis

In many cell types ER Ca^{2+} is sensed by ER resident proteins belonging to the STIM family, which monitor Ca^{2+} store content via an ER-luminal low affinity EF-hand domain. When ER Ca^{2+} is significantly lower than the Ca^{2+} affinity of STIM's Ca^{2+} binding domain, the unoccupied EF hand of STIM drives a conformational change that induces STIM clustering and activation (Liou et al., 2005; Zhang et al., 2005). This process is also strongly favored at warmer versus colder temperatures (Xiao et al., 2011; Yarotskyy and Dirksen, 2012) making it an attractive candidate for controlling the feedback between axonal ER Ca^{2+} and synaptic function. Although in immune cells activation of STIM1 leads to activation of plasma membrane Orai channels, activated STIM1 is thought to have alternate roles and different plasma membrane targets in neurons, including voltage-gated Ca^{2+} channels (Harraz and Altier, 2014; Park et al., 2010; Wang et al., 2010). Therefore, we explored whether STIM1 might be the molecular link underpinning the ER Ca^{2+} -presynaptic Ca^{2+} influx correlation (Fig 6A). We tested this idea in two ways. First we examined whether ER Ca^{2+} content remains correlated with AP-driven Ca^{2+} in flux in cells in which STIM1 expression was

ablated. We co-expressed ER-GCaMP6-150 and jRCaMP1b with an shRNA targeting STIM1 that depleted STIM1 by ~80% (see methods; Fig. S5A, B) and measured axonal $[Ca^{2+}]_{ER}$ and cytosolic 1AP-evoked Ca^{2+} signals. Remarkably, loss of STIM1 eliminated the correlation between ER Ca^{2+} content and AP-driven Ca^{2+} influx (Fig. S6B; Spearman's correlation coefficient ρ=-0.1; n.s. p=0.97) and no longer resembled a simple saturable relationship, even when the data are binned (Fig. 6B), establishing that STIM1 plays a key role in the proposed feedback loop. Second, we examined how both AP-driven Ca^{2+} influx and exocytosis are impacted by ER Ca^{2+} depletion in neurons that lack STIM1. We co-expressed GCaMP6f (Fig. 7A) or vGlut-pH (Fig. 7B) with or without the shRNA targeting STIM1 and measured single AP-driven Ca^{2+} influx before and after CPA. We found that STIM1-KD neurons were almost completely resistant to CPA-induced changes in presynaptic function whether analyzed as fractional or absolute changes induced by CPA (Fig. 7A, Control n=16, CPA effect=-0.34 ± 0.07, ***p= 0.0016; STIM1-KD n=14, CPA effect=-0.09 ± 0.05, n.s, p=0.60; see also supplementary table S2). Loss of STIM1 did not impact resting cytosolic $[Ca^{2+}]$, axonal $[Ca^{2+}]_{ER}$ or its ability to be depleted during CPA treatment (Fig. S5C-G). Furthermore, loss of CPA sensitivity was restored by re-expression of an shRNA-resistant variant of wild-type STIM1 ($STIM1^{wt}$ n=10, CPA effect=-0.31 ± 0.07, *p= 0.02). Having established that STIM1 is an essential component to mediate ER Ca^{2+} content control of presynaptic function we sought to determine if it requires the integrity of the Ca^{2+}-sensing EF hand of STIM1 that is in the ER lumen. In order to determine this we attempted to rescue STIM1-KD neurons using a variant in which the critical Ca^{2+} coordinating residues of the EF hand were mutated (Liou et al., 2005; Zhang et al., 2005) (D76A and E87A, $STIM1^{EF}$) and examined the impact on CPA-mediated reduction of presynaptic Ca^{2+} influx. In contrast to the experiments performed with $STIM1^{wt}$, expressing $STIM1^{EF}$ in STIM1 KD neurons (which correctly targets to axons, not shown) did not restore CPA-mediated changes in presynaptic Ca^{2+} influx ($STIM1^{EF}$ n=9, CPA effect=0.19 ± 0.10, $^{n.s.}$ p= 0.15), indicating that STIM1's ability to sense ER Ca^{2+} concentration is essential for driving the feedback loop observed during ER Ca^{2+} depletion (Fig. 7A, C). We also confirmed the role of STIM1 function in the reduction of activity-driven exocytosis during ER Ca^{2+} depletion by studying single AP responses of vG-pH under the same conditions (Fig. 7B, D). As expected, whereas STIM1-KD neurons do not present CPA-induced modulation of vesicle fusion (STIM1-KD, n=8, CPA effect=+0.14 ± 0.09, $^{n.s.}$ p= 0.23), restored expression of $STIM1^{wt}$ rescues the effect ($STIM1^{wt}$ n=7, CPA effect=-0.30 ± 0.04, *p= 0.031) but only if STIM1 EF-hand Ca^{2+} binding sites are functional ($STIM1^{EF}$ n=7, CPA effect=+0.11 ± 0.11, $^{n.s.}$ p= 0.54). Manipulations in STIM1 did not significantly impact basal release probability although they did result in increased AP-evoked Ca^{2+} influx in the case of the STIM1-KD (Table S2). Although STIM1 has been shown to inhibit somatic L-type Ca^{2+} channels in neurons (Park et al., 2010; Wang et al., 2010), we find little evidence for their role in presynaptic Ca^{2+} influx as these signals are insensitive to the L-type calcium channel inhibitor isradipine (n=5, effect=-0.07 ± 0.03, n.s. p= 0.80) in agreement with previously published studies (Eggermann et al., 2012). Furthermore, the increase in presynaptic AP-evoked Ca^{2+} influx in STIM1-KD neurons was not due to a selective increase in the participation of a specific type of Cav2, as the relative sensitivity of these signals to both agatoxin or conotoxin (targeting Cav2.1 and Cav2.2 respectively) was similar to control neurons (WT, n=6, aga effect=-0.57 ± 0.04, STIM1-KD,

n=10, ω-Aga effect=-0.72 ± 0.04, n.s. p= 0.21; WT, n=4, conotoxin effect=-0.73 ± 0.05, STIM1-KD, n=7, ω-Cono effect=-0.51 ± 0.06, n.s. p= 0.08).

Presynaptic STIM1 is enriched in resting nerve terminals and becomes further enriched during ER Ca^{2+} depletion

Although our data indicates that STIM1 mediates a feedback loop linking ER Ca^{2+} and presynaptic function, our experiments did not explore whether this feedback is localized to nerve terminals. To examine this we coexpressed STIM1-RFP and synapsin-GFP in individual neurons and examined their colocalization before and after ER Ca^{2+} depletion. Although STIM1-RFP is broadly distributed throughout axonal ER (Fig 8A), analysis of the local cross-correlation of STIM1-RFP with respect to synapsin-GFP fluorescence revealed that under resting conditions STIM1-RFP is enriched in nerve terminals (Fig 8B, D). This enrichment is consistent with the fact that the average value of $[Ca^{2+}]_{ER}$ (~ 150 μM) is reasonably close to the reported value of the affinity constant for Ca^{2+} binding to STIM1 (~180 μM, (Luik et al., 2008) and would predict that on average STIM1 would be in a partially activated state and thus recruited to interact with local plasma membrane binding partners. Furthermore, STIM1 presynaptic enrichment increased following ER Ca^{2+} depletion (Fig 8D-F; Cross-correlation values; Control=0.66 ± 0.03, CPA=0.75 ± 0.02; ** p=0.0012) strengthening the idea that it provides a local feedback loop at the individual synapse level.

Local STIM1 inhibits AP-evoked Ca^{2+} influx

Our analysis of presynaptic Ca^{2+} influx in STIM1 KD neurons suggests that even under resting conditions STIM1 is partially inhibiting presynaptic function. Furthermore, although we find that on average STIM1-RFP is enriched in resting nerve terminals, there is considerable variation in the relative abundance of STIM1-RFP across individual nerve terminals (Fig. 8A). This variation suggests that nerve terminals might be in a differentially-inhibited state even at rest. To test this hypothesis, we co-expressed STIM-RFP and the genetically-encoded, presynaptically-targeted Ca^{2+} indicator synaptophysin-GCaMP6f (Phy-GCaMP6) and examined the correlation between the magnitude of AP-evoked Ca^{2+} influx and the local abundance of STIM1-RFP. On average, expression of STIM1-RFP lead to a ~ 50% inhibition of single AP-evoked Ca^{2+} influx compared to neurons transfected only with Phy-GCaMP6f (Figure. 8G). These experiments also revealed a striking inverse correlation as illustrated by the example shown in Fig 8H, I of 3 en-passant synapses along the same axon: higher abundance of STIM1-RFP was associated with synapses with a lower Ca^{2+} influx, while lower abundance of STIM1-RFP was associated with larger presynaptic Ca^{2+} influx. This trend was borne out in a global analysis across a large population of boutons (564) across numerous neurons (10) and showed a strong inverse relationship between local STIM1-RFP abundance and AP-evoked Ca^{2+} influx (Fig. 8J).

DISCUSSION

Modulation of nerve terminal Ca^{2+} influx is a potent lever for controlling neurotransmitter release as the coupling between these processes is non-linear (Schneggenburger and Neher, 2000). Our detailed measurements of $[Ca^{2+}]_{ER}$ dynamics uncovered a new control system

that impacts presynaptic efficacy via a novel pathway whereby the status of $[Ca^{2+}]_{ER}$, monitored by the ER Ca^{2+} sensing protein STIM1, controls AP-driven Ca^{2+} influx. The similarity of our observations with previous characterizations of presynaptic modulation after SERCA block in both acute (Liang et al., 2002) and organotypic neuronal slices (Emptage et al., 2001) at warm temperatures suggests that this ER Ca^{2+} based control of nerve terminal function is likely ubiquitous. Given that neuronal ER Ca^{2+} dyshomeostasis is proposed to be a pathological feature of many neurological disorders including Alzheimer's disease, amyotrophic lateral sclerosis (ALS) and Parkinson's disease (Bezprozvanny, 2009; Mekahli et al., 2011; Roussel et al., 2013; Stutzmann and Mattson, 2011) our data demonstrate a new link between ER dysfunction and synaptic dysfunction. It has long been speculated that ER Ca^{2+} handling is tightly associated with the control of mitochondrial ATP production (Csordás and Hajnoczky, 2009; Szabadkai and Duchen, 2008) and that the inability of mitochondria to produce ATP contributes significantly to the pathogenesis of many neurological disorders (Mattson et al., 2008). It is possible that the feedback loop we discovered here offers a protective mechanism that tamps presynaptic activity to reduce its corresponding energetic burden (Rangaraju et al., 2014) when ER function is compromised.

The protocols and measurement approaches described in this work should prove useful in examining the molecular basis of neuronal disease states associated with ER Ca^{2+} dyshomeostasis. Previous approaches for ER Ca^{2+} measurements (in cell somas) typically required manipulations that impact function (Alonso et al., 1998; Solovyova et al., 2002; Wu et al., 2013) or used genetically-encoded Ca^{2+} indicators with insufficient sensitivity to detect axonal ER Ca^{2+} responses, including D1ER, LAR-GECO1 or G-CEPIA1er (Palmer et al., 2004; Suzuki et al., 2014; Wu et al., 2014). In contrast, ER-GCaMP6-150 and ER-GCaMP6-210 appear optimal for ER Ca^{2+} measurements as their affinities are matched to resting $[Ca^{2+}]_{ER}$ and present remarkably high responsiveness. The unique properties of these probes allowed us to explore axonal ER Ca^{2+} handling's role and established several important aspects of axonal ER behavior: (1) neuronal activity drives net axonal ER Ca^{2+} uptake but not release, contrary to what has been hypothesized in previous work (Bouchard et al., 2003; Emptage et al., 2001; Liang et al., 2002; Nizami et al., 2010; Verkhratsky, 2005; Zhang et al., 2009), (2) axonal ER Ca^{2+} fluxes do not impact synaptic cytosolic Ca^{2+} levels except during prolonged activity, (3) decreases in axonal ER Ca^{2+} content trigger a temperature-dependent feedback loop that controls neurotransmitter release and (4) this process is completely dependent on STIM1 and its ability to monitor neuronal ER Ca^{2+} content via its EF hands.

Several pieces of evidence support this novel role for STIM1. First, our estimates of resting $[Ca^{2+}]_{ER}$ suggest that changes in ER Ca^{2+} are poised to drive changes in STIM1 function since the estimates of EF hand affinity for Ca^{2+} binding in STIM1 (~ 180 μM,(Luik et al., 2008)) are very similar to our estimates of neuronal $[Ca^{2+}]_{ER}$ (~ 150 μM). Second, although in most cell types the apo-state of STIM1 drives an interaction that leads to the opening of plasma membrane Orai Ca^{2+} channels to replenish store Ca^{2+} content (Hogan and Rao, 2015), the role that such store-operated calcium entry (SOCE) plays in neurons is unclear since continuous activity-driven Ca^{2+} entry should provide sufficient cytosolic Ca^{2+} to replenish Ca^{2+} depleted stores (Moccia et al., 2015; Putney, 2003). Our work demonstrates net Ca^{2+} uptake into the ER during activity, consistent with this view. Furthermore, genetic

deletion of STIM1 in neurons does not impair SOCE (Berna-Erro et al., 2009) even though neuronal ER Ca^{2+} depletion induces STIM1 clustering (Keil et al., 2010; Klejman et al., 2009). These results all support the notion that STIM1 activation in neurons has an alternate role when acting as an ER Ca^{2+} sensor (Harraz and Altier, 2014; Hooper et al., 2013; Majewski and Kuznicki, 2015; Moreno and Vaca, 2011). Third, STIM1 activation has been shown to be strongly favored at physiological versus colder temperatures (Xiao et al., 2011; Yarotskyy and Dirksen, 2012). Congruently, presynaptic function modulation during ER Ca^{2+} depletion is also highly temperature-sensitive, while the ER Ca^{2+} depletion is not, suggesting that cold temperatures could affect the extent of STIM1 activation and impair its capacity to drive the feedback loop. Conditional and tissue specific genetic ablation of STIM1 in brain previously demonstrated that STIM1 is necessary for normal CNS function: forebrain STIM1 conditional knockout mice present significant learning defects (Garcia-Alvarez et al., 2015) and deletion of STIM1 in Purkinje neurons impairs cerebellar motor behavior (Hartmann et al., 2014). Given that STIM1 in neurons does not appear to be involved in SOCE (Berna-Erro et al., 2009), we speculate that the STIM1-mediated feedback onto the plasma membrane discovered here could be a regulatory process needed for normal neuronal and brain function.

It will be interesting in the future to elucidate mechanistic details of STIM1's control of Ca^{2+} influx and exocytosis and in particular to identify PM protein partners that allow STIM1 to control synaptic function during ER Ca^{2+} depletion, as several hypothetical PM targets are good candidates. STIM1 has been shown to interact with the C terminus of Cav1 VGCC channels in neurons to suppress depolarization-induced channel opening during ER Ca^{2+} depletion (Park et al., 2010). Since it is unlikely that such putative interaction with Cav2 VGCCs would occur in the active zone, it would require Cav2 VGCCs to be sufficiently mobile to allow access to ER-PM junctions in order for STIM1 activation to drive Ca^{2+} influx inhibition via this mechanism. The latter possibility is supported by recent studies indicating that Cav2.1 and Cav2.2 are mobile and do not reside exclusively in the active zone (Heine et al., 2016; Schneider et al., 2015). Thus, activated STIM1 could potentially provide a trap that on average would increase the distance between vesicle release sensors and Ca^{2+} entry sites, in turn inhibiting neurotransmitter release. In this regard, it is interesting to note that the relationship in between changes in Ca^{2+} entry and exocytosis after CPA is not as steep as one would predict since the ~ 35% inhibition of AP-driven presynaptic Ca^{2+} entry after CPA application led to only a ~45% inhibition of exocytosis. Furthermore removal of STIM1 led to a significant increase in Ca^{2+} influx without a corresponding change in exocytosis. This suggests that following ER Ca^{2+} depletion the effective coupling of Cav2 channels to neurotransmitter release was altered and that STIM1 may play a role in controlling channels that are biased away from release sites. Alternatively, ER Ca^{2+} depletion could drive the interaction of STIM1 with other PM partners that alter phospho-inositol levels as has been suggested at certain ER-PM contacts (Saheki et al., 2016), which in turn could impact voltage-gated K^+, Na^+ or Ca^{2+} channel function. The fact that we see considerable heterogeneity in the local presynaptic abundance of STIM1-RFP suggests that additional local factors may in turn control the localization of STIM1 in presynaptic terminals.

Our results establish new principles of neuronal ER Ca^{2+} biology and synaptic function: presynaptic ER acts as a Ca^{2+} buffer during electrical activity but it also mediates a potent feedback loop acting on the plasma membrane that controls neurotransmitter release in a process mediated by the ER Ca^{2+} sensing protein STIM1. Additionally, the new generation of tools we introduce here should open new avenues for studying ER Ca^{2+} handling in numerous subcellular locales and tissues. This should be particularly useful to dissect the molecular basis for the control of ER Ca^{2+} and to identify the sources of variability in this parameter across different neurons, helping to understand the molecular basis of the many disease states associated with ER Ca^{2+} dyshomeostasis.

STAR METHODS

CONTACT FOR REAGENT AND RESOURCE SHARING

Further information and requests for resources and reagents should be directed to and will be fulfilled by the Lead Contact Timothy A. Ryan at taryan@med.cornell.edu.

EXPERIMENTAL MODEL AND SUBJECT DETAILS

Animals—All animal-related experiments were performed in accordance with protocols approved by the Weill Cornell Medicine IACUC. Wild-type rats were of the Sprague-Dawley strain (Charles River Strain code: 400, RRID: RGD_734476).

Primary Neuronal Culture—Hippocampal CA1-CA3 neurons were isolated from 1- to 3-day-old rats of mixed gender, plated on poly-ornithine-coated coverslips, transfected 7 days after plating, and imaged 14–21 days after plating as previously described. Neurons were maintained in culture media composed of MEM (Thermofisher Scientific S1200038), 0.6% glucose, 0.1 gm/l bovine transferrin (Millipore 616420), 0.25 gm/l insulin, 0.3 gm/l glutamine, 5–10% fetal bovine serum (Atlanta Biologicals S11510), 2% B-27 (Thermofisher Scientific 17504-044), and 4 μM cytosine β-d-arabinofuranoside. Cultures were incubated at 37°C in a 95% air/5% CO2 humidified incubator for 14–21 days prior to use.

METHOD DETAILS

Replication—Not applicable

Strategy for randomization and/or stratification—Not applicable

Blinding at any stage of the study—Analysis was not blinded to genotype

Sample-size estimation and statistical method of computation—Not applicable

Inclusion and exclusion criteria of any data or subjects—Fluorescence ER Ca2+ signals in response to electrical activity (ΔF) were normalized to the resting fluorescence (F_0). The F_0 value was additionally corrected for background autofluorescence measured in a nearby non-transfected region. To avoid overestimating $\Delta F/F_0$ which would arise in neurons with low F_0 values, we set an arbitrary threshold such that F_0/background > 1.25 to

be included for further analysis. This threshold included 86.5% of all neurons tested in this study (64/74).

Reagents—All chemicals were obtained from Sigma except for cyclopiazonic acid (CPA (Alomone), thapsigargin and 1,4-dihydroxy-2,5-di-tert-butylbenzene (BHQ, Tocris), Fluo-5F, AM (Invitrogen), ionomycin (Alomone) and VGCC blockers isradipine, ω-conotoxin-GVIA and ω-Agatoxin IVA (Alomone).

Mutagenesis and selection of low affinity variants—Engineering of low affinity GCaMP variants presented in this study (Table 1 below) is part of the Genetically-Encoded Neuronal Indicator and Effector (GENIE) Project at Janelia Research Campus. Generation, selection and purification of low affinity GCaMPs was carried out as previously described (Chen et al. 2013) and the properties of the probes as a function of Ca^{2+} and pH were obtained as follows:

pH titrations: 1.65 μl of purified protein in elution buffer (20 mm TRIS-HCl, pH 8.0, 100 mm NaCl, 100 mm imidazole) was added to 100 μl of pH titrated buffer (50mM sodium citrate, 50 mM Tris, 50mM glycine, 100mM NaCl), containing either 5mM EGTA or 50mM $CaCl_2$, in duplicate. Fluorescence was measured in 96-well Greiner Bio-One transparent fluorescence plates in a Tecan Sapphire Spectrophotometer (Tecan), at 485 nm excitation and 510 nm emission, 5 nm slits, gain = 80 V.

Ca^{2+} titrations: Calcium affinity assays were performed by mixing different volumes of zero free calcium buffer (10mM EGTA, 100mM KCl, and 50mM MOPS, pH 7.2) and 39 μM free calcium buffer (10mM CaEGTA, 100mM KCl, and 50mM MOPS, pH 7.2). Extended calcium range was performed by mixing different volumes of zero free calcium buffer (10mM NTA, 100mM KCl, and 50mM MOPS, pH 7.2) and 820 μM free calcium buffer (10mM CaNTA, 100mM KCl, and 50mM MOPS, pH 7.2). Measurements were performed by adding 1.2 uL of protein (~100 μM) to 100 μl of varying buffer ratios and measuring fluorescence in 96-well Greiner Bio-One transparent fluorescence plates in a Tecan Sapphire Spectrophotometer (Tecan), at 485 nm excitation and 510 nm emission, 5 nm slits, gain = 80 V.

Gene constructs—To generate ER-GCaMPs and ER-pHluorin, selected low affinity GCaMP variants and pHluorin were targeted to the ER by adding a modified N-terminus signal peptide from human calreticulin (MGLLSVPLLLGLLGLAVA-) followed by a short linker (TGGG) and a C-terminus KDEL retention motif preceded by a short linker (GGSAGGG). All variants present a Kozak sequence (GCCGCCACC) before the initial ATG. Nucleotide sequences containing ER targeting and GCaMPs/pHluorin were optimized *in silico* for mouse protein expression, synthesized *in vitro* (Life Technologies) and cloned into the BamHI and EcoRI sites of the CaMKII promoter vector, which was a gift from Edward Boyden (Addgene plasmid #22217). G-CEPIA1er was a gift from Masamitsu Iino (Addgene plasmid # 58215). The following Kozak sequence: GCCGCCACC. STIM1-shRNA vector was obtained from Origene (#TR707032C) and uses the RNAi-targeting sequence GGATAATGGCTCTATTGGTGAGGAGACAG. STIM1-myc construct (Oh-Hora et al., 2008) was a gift from Anjana Rao (Addgene plasmid # 17732) and was used as a

template for generating an shRNA-resistant version of STIM1 and the D76A-E87A EF-mutant using site-directed mutagenesis (Agilent Technologies) as previously described (de Juan-Sanz et al., 2013). STIM1-RFP construct (Calloway et al., 2009) was a gift from Barbara A. Baird and David Holowka (Cornell University). Synaptophysin-GCaMP6f (phy-GCaMP6) was generated by adding GCaMP6f to the C-terminus of the mouse sequence of synaptophysin as previously reported (Kim and Ryan, 2013). Synapsin-GFP and VAMP-mCherry were previously cloned in the laboratory (Chi et al., 2001; Hoppa et al., 2012). To facilitate co-expression of STIM1-KD shRNA and ER-GCaMP6-150 in experiments that required triple transfections, a U6 promoter and its following shRNA sequence targeting STIM1 were amplified by PCR and cloned into a single PciI site on the ER-GCaMP6-150 vector.

Live cell imaging—Calcium phosphate-mediated gene transfer was used to transfect 6–8-day-old cultures as described previously (Sankaranarayanan et al., 2000). Live-cell imaging was performed using a custom-built laser illuminated epifluorescence microscope with an Andor iXon+ (model #DU-897E-BV) back-illuminated electron-multiplying charge-coupled device camera. Experiments were performed at a clamped temperature of 37°C (or 26°C when noticed) using a custom-built objective heater under feedback control. Action potentials were evoked by passing 1-ms current pulses, yielding fields of approximately 10 V cm^{-1} via platinum-iridium electrodes. Cells were continuously perfused at 0.1 ml min^{-1} with a Tyrode's solution containing (in mM) 119 NaCl, 2.5 KCl, 1.2 $CaCl_2$, 2.8 $MgCl_2$, 30 glucose, 10 μM 6-cyano-7-nitroquinoxaline-2,3-dione (CNQX) and 50 μM D,L-2-amino-5-phosphonovaleric acid (AP5), buffered to pH 7.4 using 25 mM HEPES. In the case of single AP vGlut1-pHluorin (vG-pH) experiments, $CaCl_2$ was increased to 2mM and $MgCl_2$ reduced to 2mM to facilitate exocytosis and improve signal-to-noise (Ariel et al., 2012; Voglmaier et al., 2006). vG-pH signals are reported as a percentage of the total vesicle pool, which fluorescence is obtained by perfusion of a Tyrode's solution containing 50mM NH_4Cl buffered at pH 7.4 using 25mM HEPES (Sankaranarayanan et al., 2000). In the case of single AP jRCaMP1b experiments, $CaCl_2$ was increased to 4mM and $MgCl_2$ reduced to 0mM to improve signal-to-noise. During experiments cells were allowed to rest for ~60 s between single action potential trials and at least 5 min between 20–100 action potential bursts. In order to obtain robust estimates for vG-pH, GCaMP6f, Fluo-5F AM, jRCaMP1b and ER-GCaMP6-210 single AP signals, responses were averaged over several trials performed every 60s (vG-pH, 12; GCaMP6f, 8–10; Fluo-5F AM, 1–3; jRCaMP1b, 10–12; ER-GCaMP6-210, 15). In the case of CPA or Thapsigargin treatments in neurons expressing GCaMP6f or vG-pH, cells were treated during 5min with a SERCA blocker and then assayed for single AP responses every 60s during the next 10–12 minutes of treatment, showing the final effect as the average of those trials during treatment. Cytosolic calcium (both Fluo-5F AM and GCaMP6f) experiments were imaged at 50Hz whereas vG-pH experiments were imaged at 10Hz. Fluo-5F AM measurements were performed by loading cells with 1 μg Fluo-5F AM at 37°C for 10 min followed by a 10 min wash and approximately 5 min equilibration at 37°C. In Fluo-5F AM experiments AP-driven Ca^{2+} entry signals and changes associated with CPA treatment are reported as ΔF signals since we observed a small increase in baseline fluorescence during SERCA blockade that arose primarily from surrounding dendrites. Using GCaMP6f in individual neurons we confirmed

that axonal baseline fluorescence is not impacted during SERCA blockade (Fig. S1A, B) and confirmed the CPA effect on single-AP stimulated Ca^{2+} entry (Fig. 1C). High resolution images of ER-targeted low-affinity GCaMP variants in live neurons were acquired using a Zeiss 63x (0.75NA) LD Plan-Neofluar objective in an inverted Zeiss LSM 880 laser scanning confocal microscope with AiryScan.

Image Analysis—Images were analyzed using the Image J plugin Time Series Analyzer V3 where typically 10–20 regions of interest (ROIs) corresponding to synaptic boutons, axonal regions or cell somas as appropriate were selected and the fluorescence was measured over time. All fitting was done with OriginPro v8. Statistical analysis was performed with OriginPro v8 and GraphPad Prism v6.0 for PC.

ER calcium dynamics analysis and imaging—ER-targeted low affinity GCaMP variants were used to measure somatic and presynaptic bouton ER Ca^{2+} dynamics. ER-GCaMP peak fluorescence ($\Delta F/F_0$) for each stimulation was found by averaging the 3 highest points divided by the average pre-stimulus fluorescence time points. ER calcium was generally imaged at 10Hz except for single AP responses (20Hz) and SERCA-block-induced ER depletion experiments (2Hz). ER calcium decay after stimulation and ER calcium depletion follow a single exponential decay, which decay constants (τ) were calculated using Origin 8.0 (LabCorp). 20AP (20Hz) experiments included in the present dataset reached at least an R-squared value of 0.95 for exponential decay fitting and a signal to noise ratio of at least 10 for the peak response over the baseline fluctuation. In addition, to avoid overestimating $\Delta F/F_0$ signals in neurons presenting low F_0 values, we set an arbitrary threshold in which F_0/background > 1.25. This threshold includes 86.5% of all neurons tested in this study (64/74).

Immunocytochemistry—To quantify endogenous STIM1 expression and measure knockdown efficiency, primary neurons expressing cytosolic GFP alone or in combination with STIM1 shRNA vector were analyzed by immunocytochemistry: after 4% PFA fixation, neurons were blocked and permeabilized for 90 min at room temperature in 0.3% Triton X-100, 10% normal goat serum and 1% BSA, and stained with antibodies overnight at 4°C against STIM1 (rabbit, Cell Signaling, #5668; 1:800) and GFP (chicken, Life Technologies, #A10262, 1:1000). Samples were then incubated for 1 hr at RT with Alexa-546 anti-rabbit and Alexa-488 anti-chicken secondary antibodies (Life Technologies). STIM1 expression levels were determined by quantifying the Alexa-546 fluorescence in somas of transfected neurons identified by GFP labeling. These values were corrected against local background staining and compared to neighboring untransfected somas to correct for variations in global staining intensity. Immunocytochemistry to ensure expression of STIM1-myc or D76A/E87A STIM1-myc in STIM1-KD neurons using an antibody against the myc tag (mouse, Abcam, #ab18185; 1:500) was performed as described previously (de Juan-Sanz et al., 2014), visualized using an Alexa-546 anti-mouse secondary antibody (Life Technologies).

QUANTIFICATION AND STATISTICAL ANALYSIS

Baseline ER Calcium estimates—We have developed two different methods for estimating ER calcium concentrations in neurons using low affinity GCaMPs.

Method 1 – Pharmacological saturation: This method relies on the experimental measurement of ER-GCaMP fluorescence at saturating $[Ca^{2+}]_{ER}$ (F_{max}), which is obtained by applying Tyrode's solution containing ionomycin at pH 6.9 buffered with 25mM HEPES. Different ionomycin concentrations were used depending on the neuronal compartment: 500μM (soma) or 50μM (axon). Knowing the *in vitro* characteristics of the indicator used (Table S1), baseline $[Ca^{2+}]_{ER}$ (Ca_r) is calculated from F_{max} using the following equation:

$$[\mathrm{Ca}]_r = K_d \left(\frac{F_r / F_{\max} - 1 / R_f}{1 - F_r / F_{\max}} \right)^{1/n} \quad \text{(Eq. 1)}$$

K_d is the affinity constant of the indicator, F_r is the measured fluorescence at rest, R_f is the dynamic range (F_{sat}/F_{apo}) and *n* is the Hill coefficient. Ionomycin application produces a change in ER pH (axons, 50μM: 7.24 to 7.35; somas 500μM: 7.24 to 7.68) that affects F_{max} depending on the pH responsiveness of the calcium-bound form of the indicator used (driven by its $pK_{a\ (sat)}$ and the Hill coefficient factor of the pH dependence). Therefore, the final F_{max} value for each indicator is corrected for a different pH variation. We have estimated the percentage contribution of pH change to fluorescence change for each indicator during ionomycin treatments and subtracted those values from F_{max} in each case before estimating ER calcium concentration. The error in the determination of $[Ca^{2+}]_{ER}$ was assumed to arise from errors associated from the measurement of the relative fluorescence change obtained in the presence of ionomycin, $f = F_{max}/F_r$ as

$$\Delta[\mathrm{Ca}]_r = \left| \frac{\partial [\mathrm{Ca}]_r}{\partial f} \right| \Delta f \quad \text{(Eq. 2)}$$

With

$$\frac{\partial [\mathrm{Ca}]_r}{\partial f} = \frac{K_d(-1+R_f)\left(\frac{f-R_f}{R_f - fR_f}\right)^{1/n}}{n(-1+f)(f-R_f)} \quad \text{(Eq. 3)}$$

We used a custom program written for Mathematica (Wolfram) to easily propagate these errors, which can be found at https://github.com/jaimedejuan/Error-propagation-ER-Ca

Method 2 – Indicator pair comparison: This method relies on measuring the same cellular response with different indicators. For a single indicator (indicator 1), the relationship between fluorescence and calcium from Eq.1 can be expressed also as:

$$\frac{F_{r(1)}}{F_{0(1)}} = 1 + (R_{f(1)} - 1) \frac{[\mathrm{Ca}]_r^{n(1)}}{K_{d(1)} + [\mathrm{Ca}]_r^{n(1)}} \quad \text{(Eq. 4)}$$

Where F_r is the fluorescence at rest, F_0 is the minimum fluorescence, R_f is the dynamic range of indicator 1, K_d is the affinity constant of the indicator 1, $[Ca]_r$ is the calcium concentration at rest and $n^{(1)}$ is the Hill coefficient of indicator 1.

After stimulation calcium has changed to a new concentration, $[Ca]_s$, which corresponds to a new fluorescence F_s. One can get the ratio of both equations obtaining:

$$\frac{F_{s(1)}}{F_{r(1)}}=\frac{1+(R_{f(1)}-1)\frac{[\mathrm{Ca}]_s^{n(1)}}{K_{d(1)}+[\mathrm{Ca}]_s^{n(1)}}}{1+(R_{f(1)}-1)\frac{[\mathrm{Ca}]_r^{n(1)}}{K_{d(1)}+[\mathrm{Ca}]_r^{n(1)}}} \quad \text{(Eq. 5)}$$

A single equation is not sufficient to solve for the values of $[Ca]_r$ and $[Ca]_s$, but the same procedure can be applied to a different indicator (indicator 2)

$$\frac{F_{s(2)}}{F_{r(2)}}=\frac{1+(R_{f(2)}-1)\frac{[\mathrm{Ca}]_s^{n(2)}}{K_{d(2)}+[\mathrm{Ca}]_s^{n(2)}}}{1+(R_{f(2)}-1)\frac{[\mathrm{Ca}]_r^{n(2)}}{K_{d(2)}+[\mathrm{Ca}]_r^{n(2)}}} \quad \text{(Eq. 6)}$$

Once fluorescence values at rest ($F_{r(1)}$ and $F_{r(2)}$) and after stimulation ($F_{s(1)}$ and $F_{s(2)}$) are obtained experimentally for the two indicators, the system formed by Eqs. (3) and (4) contains only two unknowns $[Ca]_r$ and $[Ca]_s$, and values for these can be found numerically with the Newton method. This was done with a custom program written for Mathematica (Wolfram), which can be found at https://github.com/jaimedejuan/pair-wise-indicator-calcium.git

Cytosolic calcium analysis using GCaMP6f or jRCaMP1b—GCaMP6f and jRCaMP1b have nonlinear responses to changes in cytosolic $[Ca^{2+}]$ as previously described *in vitro* (Chen et al., 2013). To linearize GCaMP6f and jRCaMP1b signals we inverted the Hill equation of fluorescence vs $[Ca^{2+}]$ and used the known *in vitro* parameters of these indicators to estimate nM changes during activity. Similarly to μM estimates in ER $[Ca^{2+}]$, this conversion relies on the experimental measurement of GCaMP6f and jRCaMP1b fluorescence at saturating $[Ca^{2+}]$, which is obtained by applying Tyrode's solution containing 1 μM ionomycin at pH 6.9 (F_{max}) as previously reported (Hoppa et al., 2012). Baseline cytosolic Ca^{2+} ($[Ca]_{cyto}$) is calculated from F_{max} using the following equation:

$$[\mathrm{Ca}]_{\mathrm{cyto}}=K_d\left(\frac{F_{\mathrm{cyto}}/F_{\mathrm{max}}-1/R_f}{1-F_{\mathrm{cyto}}/F_{\mathrm{max}}}\right)^{1/n} \quad \text{(Eq. 7)}$$

Where K_d is the affinity constant of the indicator, F_{cyto} is the fluorescence measured at rest, R_f is the dynamic range (F_{sat}/F_{apo}) and n is the Hill coefficient. In general, linearized

$[Ca^{2+}]_{cyto}$ (nM) signals are shown in this study as normalized traces to show percentage effects more clearly.. In experiments were prolonged stimulation was used, 1 μM ionomycin perfusion was used as a control to ensure that activity-driven responses were not limited by indicator saturation (Fig. S4B, C).

ER pH measurements—ER pH measurements were made using ER-targeted pHluorin (pKa 7.1) expressed in neurons and imaged at neuronal somas or presynaptic varicosities identified by VAMP-mCherry expression. Neurons were briefly perfused with a Tyrode's solution containing 100mM NH_4Cl buffered at pH 7.4 and 7.8 using 25mM HEPES, which equilibrated ER pH to 7.4 or 7.8 after a transient overshoot of fluorescence (Fig. S2C) as previously described (Kim et al., 1998). The fluorescence value when pH stabilizes at 7.4 or 7.8 allows estimating resting ER pH (Fig. S2D) value using the modified Henderson-Hasselbalch equation:

$$pH = pK_a - \log\left[\left(\frac{1+10^{pK_a - pH(NH_4Cl)}}{\frac{F_0}{F_{NH_4Cl}}}\right) - 1\right] \quad \text{(Eq. 8)}$$

pK_a is the pK_a of pHluorin, 7.1, pH(NH_4Cl) is the pH of 100mM NH_4Cl buffer used, F_0 is the fluorescence of ER pHluorin measured before NH_4Cl perfusion, F_{NH4Cl} is the fluorescence of ER pHluorin measured upon NH_4Cl perfusion when signal is stable. Final pH value obtained per cell is the average of 7.4- and 7.8-based estimates.

Analysis of correlation between $[Ca^{2+}]_{ER}$ and single AP Ca^{2+} entry—To examine the putative correlation between $[Ca^{2+}]_{ER}$ and single AP Ca^{2+} entry we assumed a monotonic relationship between the two variables and calculated the Spearman's correlation coefficient (ρ) of our raw data sets (presented in Fig. S6A, B) using R (R Development Core Team). To reduce observational noise, we binned our raw data using a bin size of $[Ca^{2+}]_{ER}$ = 25 μM starting from 75 μM. Errors of binned data points for $[Ca^{2+}]_{ER}$ and 1AP jRCaMP1b responses were calculated by summing in quadrature the experimental estimates of the error for each individual data point. We used the binned data set (presented in Figure 6) to fit our data with better accuracy. A Hill equation fit was selected because 1) reported less error in the determination of the equation parameters as well as a better adjusted R-square value (Adj R-sq= 0.87) and 2) is in agreement with previously published studies showing that STIM1 activation presents high cooperativity well described by a Hill equation (Luik et al., 2008; Stathopulos et al., 2008; Zheng et al., 2011). The Hill model was fitted with statistical weights using Origin 8.0 (LabCorp).

Estimates of contributions of ER efflux to resting cytosolic Ca^{2+}—Although signals in axons are small the reported affinity of GCaMP6f (Kd= 375 nM) should be in the correct range to asses changes in resting calcium. Our procedures used to linearize the GCaMP6f response also allow us to estimate the resting Ca since we know the in-vitro properties of the indicator. These calculations predict that the resting Ca^{2+} concentration in axons is ~120 nM (in both axons and dendrites). One can then ask how large the fluctuations are in the baseline to get a sense of how much the signal would have to change in order to

see something meaningful. The standard deviation of the baseline (Fig S1D) represents a ΔF/F ~ 0.01 and corresponds to a fluctuation of resting Ca of ~ 1.1 nM. By comparison a single AP transiently elevates the average bouton Ca^{2+} to 9.6 nM (ΔF/F signal ~0.07), and the CPA induced changes in the dendrite correspond to an elevation of 11.8 nM (ΔF/F= 0.08). This demonstrates that GCaMP6f is easily capable of detecting similar changes in axons and, therefore, we feel it is justified to conclude that SERCA block does not result in increased baseline cytosolic calcium in the axon. We suspect that the difference observed is a consequence of a different ratio between ER volume and cytoplasmic volume - whereas dendrites likely have elaborated ER networks, axonal ER appears to be much simpler and might occupy less % of the total cytoplasmic volume.

Statistics—Error bars indicate mean ± S.E.M. Box whisker plots represent median (line), mean (point), 25 – 75 percentile (box), 10 – 90 percentile (whisker), 1 – 99 percentile (X) and min - max (−) ranges. Statistical analyses were performed by one-way ANOVA followed by Tukey's multiple comparisons test except for paired data (e.g., before and after CPA) where paired t-test was used to compare. When analyzing correlation, the Spearman's correlation coefficient (ρ) was considered significant if $p<0.05$. $P < 0.05$ was considered significant and denoted with a single asterisk, whereas $P < 0.01$, $P<0.001$ and $P < 0.0001$ are denoted with two, three, and four asterisks, respectively. The sample replicate number (n) referred to in all figures represents individual cells of a given treatment condition.

DATA AND SOFTWARE AVAILABILITY

A custom program written for Mathematica (Wolfram) to easily propagate errors on ionomycin-based ER calcium estimates can be found at https://github.com/jaimedejuan/Error-propagation-ER-Ca

A custom program written for Mathematica (Wolfram) to estimate baseline ER calcium by comparing responses from 2 different indicators can be found at https://github.com/jaimedejuan/pair-wise-indicator-calcium.git

The Image J plugin Time Series Analyzer V3 is available at https://imagej.nih.gov/ij/plugins/time-series.html

Supplementary Material

Refer to Web version on PubMed Central for supplementary material.

Acknowledgments

This work was supported by a grant from the NIH (NS036942) to TAR. We thank Loren L. Looger and Jeremy Dittman for comments and Julia Marrs and Lucia A. Saidenberg for technical assistance. We thank the members of the Ryan lab for helpful discussion, especially Nimra Asi for her additional contribution to the statistical analysis.

REFERENCES

Alonso MT, Barrero MJ, Carnicero E, Montero M, Garcia-Sancho J, Alvarez J. Functional measurements of [Ca2+] in the endoplasmic reticulum using a herpes virus to deliver targeted aequorin. Cell Calcium. 1998; 24:87–96. [PubMed: 9803309]

Ariel P, Hoppa MB, Ryan TA. Intrinsic variability in Pv, RRP size, Ca(2+) channel repertoire, and presynaptic potentiation in individual synaptic boutons. Front Synaptic Neurosci. 2012; 4:9. [PubMed: 23335896]

Armbruster M, Ryan TA. Synaptic vesicle retrieval time is a cell-wide rather than individual-synapse property. Nat Neurosci. 2011; 14:824–826. [PubMed: 21623361]

Beck A, Lohr C, Deitmer JW. Calcium transients in subcompartments of the leech Retzius neuron as induced by single action potentials. J Neurobiol. 2001; 48:1–18. [PubMed: 11391646]

Berna-Erro A, Braun A, Kraft R, Kleinschnitz C, Schuhmann MK, Stegner D, Wultsch T, Eilers J, Meuth SG, Stoll G, et al. STIM2 regulates capacitive Ca2+ entry in neurons and plays a key role in hypoxic neuronal cell death. Sci Signal. 2009; 2:ra67. [PubMed: 19843959]

Bezprozvanny I. Calcium signaling and neurodegenerative diseases. Trends Mol Med. 2009; 15:89–100. [PubMed: 19230774]

Blackstone C, O'Kane CJ, Reid E. Hereditary spastic paraplegias: membrane traffic and the motor pathway. Nat Rev Neurosci. 2011; 12:31–42. [PubMed: 21139634]

Bouchard R, Pattarini R, Geiger JD. Presence and functional significance of presynaptic ryanodine receptors. Prog Neurobiol. 2003; 69:391–418. [PubMed: 12880633]

Calloway N, Gouzer G, Xue M, Ryan TA. The active-zone protein Munc13 controls the use-dependence of presynaptic voltage-gated calcium channels. Elife. 2015; 4:e07728.

Calloway N, Vig M, Kinet JP, Holowka D, Baird B. Molecular clustering of STIM1 with Orai1/CRACM1 at the plasma membrane depends dynamically on depletion of Ca2+ stores and on electrostatic interactions. Mol Biol Cell. 2009; 20:389–399. [PubMed: 18987344]

Carter AG, Vogt KE, Foster KA, Regehr WG. Assessing the role of calcium-induced calcium release in short-term presynaptic plasticity at excitatory central synapses. J Neurosci. 2002; 22:21–28. [PubMed: 11756484]

Chen TW, Wardill TJ, Sun Y, Pulver SR, Renninger SL, Baohan A, Schreiter ER, Kerr RA, Orger MB, Jayaraman V, et al. Ultrasensitive fluorescent proteins for imaging neuronal activity. Nature. 2013; 499:295–300. [PubMed: 23868258]

Chi P, Greengard P, Ryan TA. Synapsin dispersion and reclustering during synaptic activity. Nat Neurosci. 2001; 4:1187–1193. [PubMed: 11685225]

Csordás G, Hajnóczky G. SR/ER-mitochondrial local communication: calcium and ROS. Biochim Biophys Acta. 2009; 1787:1352–1362. [PubMed: 19527680]

Dana H, Mohar B, Sun Y, Narayan S, Gordus A, Hasseman JP, Tsegaye G, Holt GT, Hu A, Walpita D, et al. Sensitive red protein calcium indicators for imaging neural activity. 2016

de Juan-Sanz J, Nunez E, López-Corcuera B, Aragón C. Constitutive endocytosis and turnover of the neuronal glycine transporter GlyT2 is dependent on ubiquitination of a C-terminal lysine cluster. PLoS One. 2013; 8:e58863. [PubMed: 23484054]

de Juan-Sanz J, Nunez E, Zafra F, Berrocal M, Corbacho I, Ibanez I, Arribas-González E, Marcos D, López-Corcuera B, Mata AM, et al. Presynaptic control of glycine transporter 2 (GlyT2) by physical and functional association with plasma membrane Ca2+-ATPase (PMCA) and Na+- Ca2+ exchanger (NCX). J Biol Chem. 2014; 289:34308–34324. [PubMed: 25315779]

Eggermann E, Bucurenciu I, Goswami SP, Jonas P. Nanodomain coupling between Ca(2+) channels and sensors of exocytosis at fast mammalian synapses. Nat Rev Neurosci. 2012; 13:7–21.

Emptage NJ, Reid CA, Fine A. Calcium stores in hippocampal synaptic boutons mediate short-term plasticity, store-operated Ca2+ entry, and spontaneous transmitter release. Neuron. 2001; 29:197–208. [PubMed: 11182091]

Foskett JK, White C, Cheung KH, Mak DO. Inositol trisphosphate receptor Ca2+ release channels. Physiol Rev. 2007; 87:593–658. [PubMed: 17429043]

Garcia-Alvarez G, Shetty MS, Lu B, Yap KA, Oh-Hora M, Sajikumar S, Bichler Z, Fivaz M. Impaired spatial memory and enhanced long-term potentiation in mice with forebrain-specific ablation of the Stim genes. Front Behav Neurosci. 2015; 9:180. [PubMed: 26236206]

Harraz OF, Altier C. STIM1-mediated bidirectional regulation of Ca(2+) entry through voltage-gated calcium channels (VGCC) and calcium-release activated channels (CRAC). Frontiers in cellular neuroscience. 2014; 8:43. [PubMed: 24605083]

Hartmann J, Karl RM, Alexander RPD, Adelsberger H, Brill MS, Rühlmann C, Ansel A, Sakimura K, Baba Y, Kurosaki T, et al. STIM1 controls neuronal Ca^{2+} signaling, mGluR1-dependent synaptic transmission, and cerebellar motor behavior. Neuron. 2014; 82:635–644. [PubMed: 24811382]

Heine M, Ciuraszkiewicz A, Voigt A, Heck J, Bikbaev A. Surface dynamics of voltage-gated ion channels. Channels (Austin). 2016:1–15.

Henderson MJ, Baldwin HA, Werley CA, Boccardo S, Whitaker LR, Yan X, Holt GT, Schreiter ER, Looger LL, Cohen AE, et al. A Low Affinity GCaMP3 Variant (GCaMPer) for Imaging the Endoplasmic Reticulum Calcium Store. PLoS One. 2015; 10:e0139273. [PubMed: 26451944]

Henkart MP, Reese TS, Brinley FJ Jr. Endoplasmic reticulum sequesters calcium in the squid giant axon. Science. 1978; 202:1300–1303. [PubMed: 725607]

Hogan PG, Rao A. Store-operated calcium entry: Mechanisms and modulation. Biochem Biophys Res Commun. 2015; 460:40–49. [PubMed: 25998732]

Hooper R, Samakai E, Kedra J, Soboloff J. Multifaceted roles of STIM proteins. Pflügers Arch, EJP. 2013; 465:1383–1396. [PubMed: 23568369]

Hoppa MB, Lana B, Margas W, Dolphin AC, Ryan TA. alpha2delta expression sets presynaptic calcium channel abundance and release probability. Nature. 2012; 486:122–125. [PubMed: 22678293]

Keil JM, Shen Z, Briggs SP, Patrick GN. Regulation of STIM1 and SOCE by the ubiquitin-proteasome system (UPS). PloS One. 2010; 5:e13465. [PubMed: 20976103]

Kendall JM, Badminton MN, Dormer RL, Campbell AK. Changes in free calcium in the endoplasmic reticulum of living cells detected using targeted aequorin. Anal Biochem. 1994; 221:173–181. [PubMed: 7985790]

Kim JH, Johannes L, Goud B, Antony C, Lingwood CA, Daneman R, Grinstein S. Noninvasive measurement of the pH of the endoplasmic reticulum at rest and during calcium release. Proc Natl Acad Sci USA. 1998:2997–3002. [PubMed: 9501204]

Kim SH, Ryan TA. Balance of Calcineurin Aalpha and CDK5 Activities Sets Release Probability at Nerve Terminals. J Neurosci. 2013; 33:8937–8950. [PubMed: 23699505]

Kiyonaka S, Kajimoto T, Sakaguchi R, Shinmi D, Omatsu-Kanbe M, Matsuura H, Imamura H, Yoshizaki T, Hamachi I, Morii T, et al. Genetically encoded fluorescent thermosensors visualize subcellular thermoregulation in living cells. Nat Methods. 2013; 10:1232–1238. [PubMed: 24122038]

Klejman ME, Gruszczynska-Biegala J, Skibinska-Kijek A, Wisniewska MB, Misztal K, Blazejczyk M, Bojarski L, Kuznicki J. Expression of STIM1 in brain and puncta-like co-localization of STIM1 and ORAI1 upon depletion of Ca(2+) store in neurons. Neurochem Int. 2009; 54:49–55. [PubMed: 19013491]

Liang Y, Yuan LL, Johnston D, Gray R. Calcium signaling at single mossy fiber presynaptic terminals in the rat hippocampus. J Neurophysiol. 2002; 87:1132–1137. [PubMed: 11826078]

Liou J, Kim ML, Heo WD, Jones JT, Myers JW, Ferrell JE Jr, Meyer T. STIM is a Ca2+ sensor essential for Ca2+-store-depletion-triggered Ca2+ influx. Curr Biol. 2005; 15:1235–1241. [PubMed: 16005298]

Liu X, Betzenhauser MJ, Reiken S, Meli AC, Xie W, Chen BX, Arancio O, Marks AR. Role of leaky neuronal ryanodine receptors in stress-induced cognitive dysfunction. Cell. 2012; 150:1055–1067. [PubMed: 22939628]

Llinas R, Sugimori M, Silver RB. Microdomains of high calcium concentration in a presynaptic terminal. Science. 1992; 256:677–679. [PubMed: 1350109]

Luik RM, Wang B, Prakriya M, Wu MM, Lewis RS. Oligomerization of STIM1 couples ER calcium depletion to CRAC channel activation. Nature. 2008; 454:538–542. [PubMed: 18596693]

Majewski L, Kuznicki J. SOCE in neurons: Signaling or just refilling? Biochim Biophys Acta. 2015; 1853:1940–1952. [PubMed: 25646572]

Mattson MP, Gleichmann M, Cheng A. Mitochondria in neuroplasticity and neurological disorders. Neuron. 2008; 60:748–766. [PubMed: 19081372]

Mekahli D, Bultynck G, Parys JB, De Smedt H, Missiaen L. Endoplasmic-reticulum calcium depletion and disease. Cold Spring Harb Perspect Biol. 2011; 3:a004317. [PubMed: 21441595]

Miyawaki A, Llopis J, Heim R, McCaffery JM, Adams JA, Ikura M, Tsien RY. Fluorescent indicators for Ca2+ based on green fluorescent proteins and calmodulin. Nature. 1997; 388:882–887. [PubMed: 9278050]

Moccia F, Estella Z, Teresa S, Franco T, Germano G, Lisa M, Francesco L, Egidio DA. Stim and Orai proteins in neuronal Ca(2+) signaling and excitability. Frontiers in cellular neuroscience. 2015; 9:153. [PubMed: 25964739]

Montenegro G, Rebelo AP, Connell J, Allison R, Babalini C, D'Aloia M, Montieri P, Schule R, Ishiura H, Price J, et al. Mutations in the ER-shaping protein reticulon 2 cause the axon-degenerative disorder hereditary spastic paraplegia type 12. J Clin Invest. 2012; 122:538–544. [PubMed: 22232211]

Moreno C, Vaca L. SOC and now also SIC: store-operated and store-inhibited channels. IUBMB life. 2011; 63:856–863. [PubMed: 21901816]

Munro S, Pelham HR. A C-terminal signal prevents secretion of luminal ER proteins. Cell. 1987; 48:899–907. [PubMed: 3545499]

Nizami S, Lee VW, Davies J, Long P, Jovanovic JN, Sihra TS. Presynaptic roles of intracellular Ca(2+) stores in signalling and exocytosis. Biochem Soc Trans. 2010; 38:529–535. [PubMed: 20298216]

Noreau A, Dion PA, Rouleau GA. Molecular aspects of hereditary spastic paraplegia. Exp Cell Res. 2014; 325:18–26. [PubMed: 24631291]

Oh-Hora M, Yamashita M, Hogan PG, Sharma S, Lamperti E, Chung W, Prakriya M, Feske S, Rao A. Dual functions for the endoplasmic reticulum calcium sensors STIM1 and STIM2 in T cell activation and tolerance. Nat Immunol. 2008; 9:432–443. [PubMed: 18327260]

Palmer AE, Jin C, Reed JC, Tsien RY. Bcl-2-mediated alterations in endoplasmic reticulum Ca2+ analyzed with an improved genetically encoded fluorescent sensor. Proc Natl Acad Sci USA. 2004; 101:17404–17409. [PubMed: 15585581]

Park CY, Shcheglovitov A, Dolmetsch R. The CRAC channel activator STIM1 binds and inhibits L-type voltage-gated calcium channels. Science. 2010; 330:101–105. [PubMed: 20929812]

Putney JW. Capacitative calcium entry in the nervous system. Cell Calcium. 2003; 34:339–344. [PubMed: 12909080]

Rangaraju V, Calloway N, Ryan TA. Activity-driven local ATP synthesis is required for synaptic function. Cell. 2014; 156:825–835. [PubMed: 24529383]

Roussel BD, Kruppa AJ, Miranda E, Crowther DC, Lomas DA, Marciniak SJ. Endoplasmic reticulum dysfunction in neurological disease. Lancet Neurol. 2013; 12:105–118. [PubMed: 23237905]

Saheki Y, Bian X, Schauder CM, Sawaki Y, Surma MA, Klose C, Pincet F, Reinisch KM, De Camilli P. Control of plasma membrane lipid homeostasis by the extended synaptotagmins. Nat Cell Biol. 2016; 18:504–515. [PubMed: 27065097]

Sankaranarayanan S, De Angelis D, Rothman JE, Ryan TA. The use of pHluorins for optical measurements of presynaptic activity. Biophys J. 2000; 79:2199–2208. [PubMed: 11023924]

Schneggenburger R, Neher E. Intracellular calcium dependence of transmitter release rates at a fast central synapse. Nature. 2000; 406:889–893. [PubMed: 10972290]

Schneider R, Hosy E, Kohl J, Klueva J, Choquet D, Thomas U, Voigt A, Heine M. Mobility of calcium channels in the presynaptic membrane. Neuron. 2015; 86:672–679. [PubMed: 25892305]

Solovyova N, Veselovsky N, Toescu E, Verkhratsky A. Ca(2+) dynamics in the lumen of the endoplasmic reticulum in sensory neurons: direct visualization of Ca(2+)-induced Ca(2+) release triggered by physiological Ca(2+) entry. EMBO J. 2002; 21:622–630. [PubMed: 11847110]

Stanley EF. The calcium channel and the organization of the presynaptic transmitter release face. Trends Neurosci. 1997; 20:404–409. [PubMed: 9292969]

Stathopulos PB, Zheng L, Li GY, Plevin MJ, Ikura M. Structural and mechanistic insights into STIM1-mediated initiation of store-operated calcium entry. Cell. 2008; 135:110–122. [PubMed: 18854159]

Stutzmann GE, Mattson MP. Endoplasmic reticulum Ca(2+) handling in excitable cells in health and disease. Pharmacol Rev. 2011; 63:700–727. [PubMed: 21737534]

Suzuki J, Kanemaru K, Ishii K, Ohkura M, Okubo Y, Iino M. Imaging intraorganellar Ca2+ at subcellular resolution using CEPIA. Nat Commun. 2014; 5:4153. [PubMed: 24923787]

Szabadkai G, Duchen MR. Mitochondria: the hub of cellular Ca2+ signaling. Physiology (Bethesda). 2008; 23:84–94. [PubMed: 18400691]

Teuling E, Ahmed S, Haasdijk E, Demmers J, Steinmetz MO, Akhmanova A, Jaarsma D, Hoogenraad CC. Motor neuron disease-associated mutant vesicle-associated membrane protein-associated protein (VAP) B recruits wild-type VAPs into endoplasmic reticulum-derived tubular aggregates. J Neurosci. 2007; 27:9801–9815. [PubMed: 17804640]

Tsukita S, Ishikawa H. Three-dimensional distribution of smooth endoplasmic reticulum in myelinated axons. J Electron Microsc (Tokyo). 1976; 25:141–149. [PubMed: 1025229]

Verkhratsky A. Physiology and pathophysiology of the calcium store in the endoplasmic reticulum of neurons. Physiol Rev. 2005; 85:201–279. [PubMed: 15618481]

Voglmaier SM, Kam K, Yang H, Fortin DL, Hua Z, Nicoll RA, Edwards RH. Distinct endocytic pathways control the rate and extent of synaptic vesicle protein recycling. Neuron. 2006; 51:71–84. [PubMed: 16815333]

Wang Y, Deng X, Mancarella S, Hendron E, Eguchi S, Soboloff J, Tang XD, Gill DL. The calcium store sensor, STIM1, reciprocally controls Orai and CaV1.2 channels. Science. 2010; 330:105–109. [PubMed: 20929813]

Wu B, Yamaguchi H, Lai FA, Shen J. Presenilins regulate calcium homeostasis and presynaptic function via ryanodine receptors in hippocampal neurons. Proc Natl Acad Sci USA. 2013; 110:15091–15096. [PubMed: 23918386]

Wu J, Prole DL, Shen Y, Lin Z, Gnanasekaran A, Liu Y, Chen L, Zhou H, Chen SR, Usachev YM, et al. Red fluorescent genetically encoded Ca2+ indicators for use in mitochondria and endoplasmic reticulum. Biochem J. 2014; 464:13–22. [PubMed: 25164254]

Xiao B, Coste B, Mathur J, Patapoutian A. Temperature-dependent STIM1 activation induces Ca^{2}+ influx and modulates gene expression. Nat Chem Biol. 2011; 7:351–358. [PubMed: 21499266]

Yarotskyy V, Dirksen R. Temperature and RyR1 Regulate the Activation Rate of Store-Operated Ca2+ Entry Current in Myotubes. Biophys J. 2012; 103:202–211. [PubMed: 22853897]

Zhang C, Wu B, Beglopoulos V, Wines-Samuelson M, Zhang D, Dragatsis I, Südhof TC, Shen J. Presenilins are essential for regulating neurotransmitter release. Nature. 2009; 460:632–636. [PubMed: 19641596]

Zhang SL, Yu Y, Roos J, Kozak JA, Deerinck TJ, Ellisman MH, Stauderman KA, Cahalan MD. STIM1 is a Ca2+ sensor that activates CRAC channels and migrates from the Ca2+ store to the plasma membrane. Nature. 2005; 437:902–905. [PubMed: 16208375]

Zheng L, Stathopulos PB, Schindl R, Li GY, Romanin C, Ikura M. Auto-inhibitory role of the EF-SAM domain of STIM proteins in store-operated calcium entry. Proc Natl Acad Sci U S A. 2011; 108:1337–1342. [PubMed: 21217057]

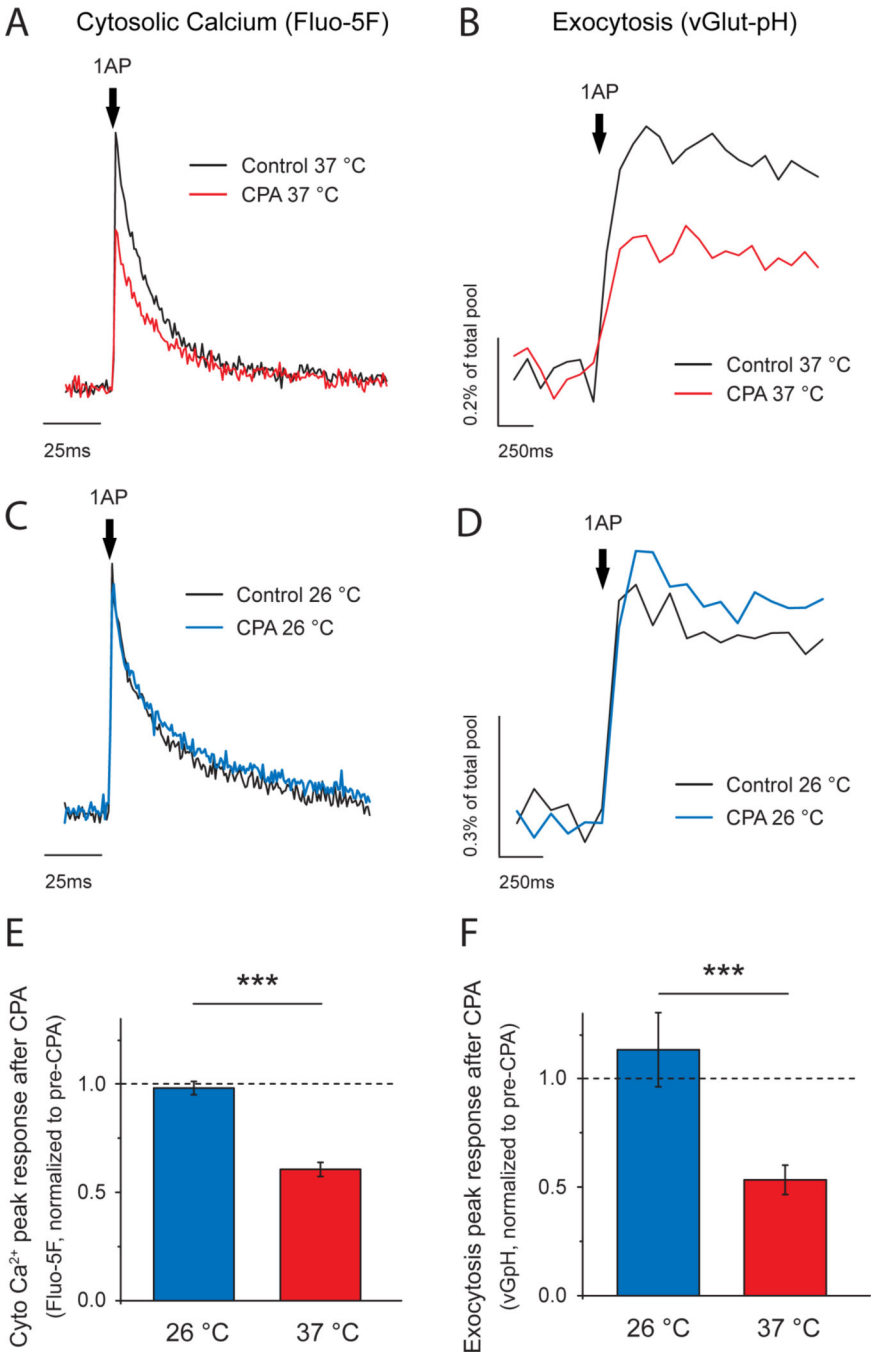

Figure 1. ER Ca^{2+} handling is critical for presynaptic function at physiological temperature

(A-D) Representative traces of single AP presynaptic cytosolic Ca^{2+} responses measured using Fluo-5F AM (A, C) and vesicular exocytosis measured using vG-pH (B, D) before and after CPA treatment. Experiments were performed at 37°C (A, B, shown in red) and 26°C (C, D, shown in blue). Fluo-5F AM traces were normalized to the pre-CPA ΔF response (black trace). vG-pH responses are shown as percentage of their maximum fluorescence, obtained by brief perfusion of NH_4Cl buffered at pH 7.4. Differential effects observed are summarized by showing the remaining response after CPA treatment in each of the

conditions (E, F): Fluo-5F AM, (26°C) n =10, (37°C) n =14; ***p=$1.44 \cdot 10^{-7}$. vG-pH, (26°C) n =7, (37°C) n =10; ***p=$2.75 \cdot 10^{-4}$.

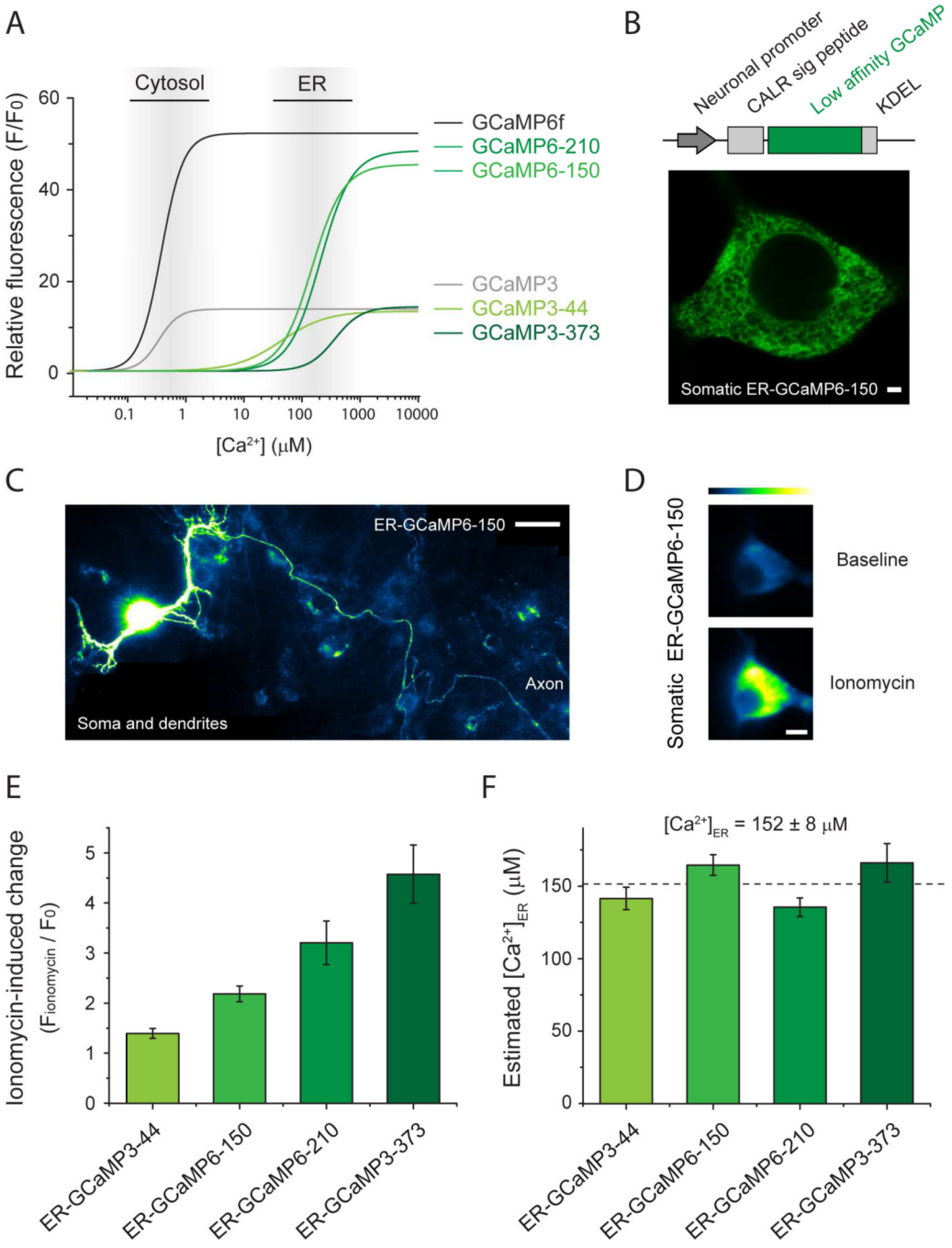

Figure 2. A new generation of ultrasensitive ER Ca^{2+} indicators

(A) Predicted relative fluorescence vs Ca^{2+} curves based on binding parameters obtained *in vitro* (Table S1) of low affinity calcium indicators GCaMP3-44, GCaMP6-150, GCaMP6-210 and GCaMP3-373 (light to dark green, high to low affinity) and high affinity cytosolic indicators GCaMP3 (grey) and GCaMP6f (black). Approximate ranges of Ca^{2+} concentration in the cytosol and ER are indicated by grey gradient boxes. (B) top: targeting scheme for expression in the neuronal ER by adding the N-terminal signal peptide of calreticulin (CALR sig peptide) and the C-terminal KDEL retention motif. Bottom: high

resolution image of somatic ER-GCaMP6-150 shows neuronal ER structure. Scale bar 2 μM. (C) Montage of several fields from a neuron expressing ER-GCaMP6-150, which localizes in the ER network in the soma, dendrites and axons. Scale bar 40 μM. (D-F) Neurons were treated with 500 μM ionomycin to induce indicator saturation for calibration. (D) Example pseudocolor images of somatic ER-GCaMP6-150 before and after ionomycin treatment. Pseudocolor scale shows low to high intensity. Scale bar 8 μM. (E) Average peak fold-change in fluorescence ($F_{ionomycin}/F_0$) during ionomycin application for each ER-GCaMP. ER-GCaMP3-44, n=14; ER-GCaMP6-150, n=8; ER-GCaMP6-210, n=9; ER-GCaMP3-373, n=8; errors are ± S.E.M. (F) pH-corrected estimate of resting ER calcium concentration based on each indicator saturation response. Dashed line indicates the average of the estimates from each of the indicators.

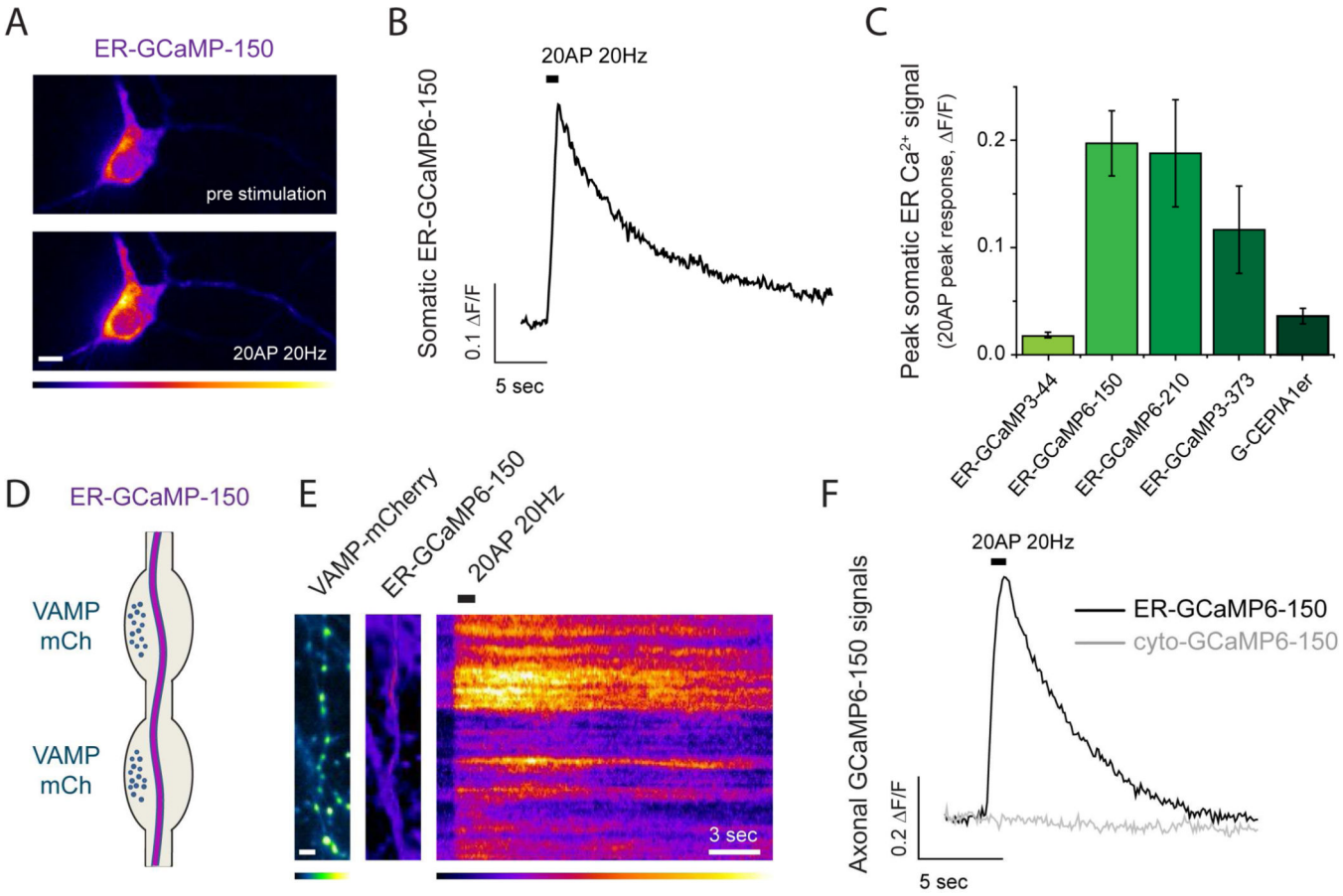

Figure 3. Neuronal activity drives ER Ca^{2+} uptake

(A-C) Somatic ER Ca^{2+} responses to 20AP (20Hz) stimulation using different indicators. (A) Representative pseudocolor images of somatic ER-GCaMP6-150 before and after 20AP (20Hz) stimulation and (B) the corresponding fluorescence intensity over time (pseudocolor scale below showing low to high intensity). Scale bar 8 μM. (C) Average of 20AP peak somatic ER-GCaMP responses: G-CEPIA1er, n=5; ER-GCaMP3-44, n=11; ER-GCaMP6-150, n=12; ER-GCaMP6-210, n=6; ER-GCaMP3-373, n=11; errors are ± S.E.M. (D) Diagram showing axonal ER crossing nerve terminals where ER Ca^{2+} responses were measured. (E) ER-GCaMP-150 signals in presynaptic boutons identified by VAMP-mCherry expression (left, colored in green; scale bar 4 μM) at rest (middle image) and during a 20 AP stimulus (displayed as a kymograph, right; pseudocolor scale shows low to high intensity). Scale bar 3 s. (F) Representative 20AP presynaptic response measured with ER-GCaMP6-150 or cytosolic GCaMP6-150 (same variant without ER-targeting sequences).

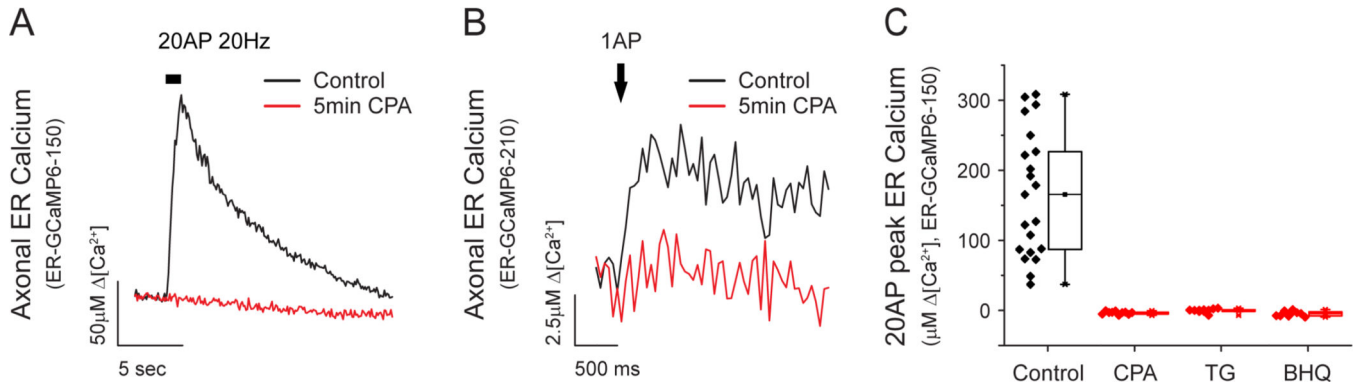

Figure 4. SERCA function is necessary for activity-driven ER Ca^{2+} uptake

(A) Representative presynaptic responses of ER-GCaMP6-150 to 20AP (20Hz) or (B) ER-GCaMP6-210 to a single AP stimulus before and after 5 min of CPA (50 μM) application (black and red, respectively). Average of single AP $\Delta[Ca^{2+}]_{ER}$ responses before CPA was 5.9 ± 1.3 μM (n=5), which was reduced to 0.2 ± 0.2 μM after CPA treatment (n=3). (C) Box plots showing average and single-cell calibrated peak responses of neurons stimulated with 20AP (20Hz) before and after 5 min of treatment with CPA (n=10), thapsigargin (TG, 1 μM, n=9) or 1,4-dihydroxy-2,5-di-tert-butylbenzene (BHQ, 50 μM, n=9).

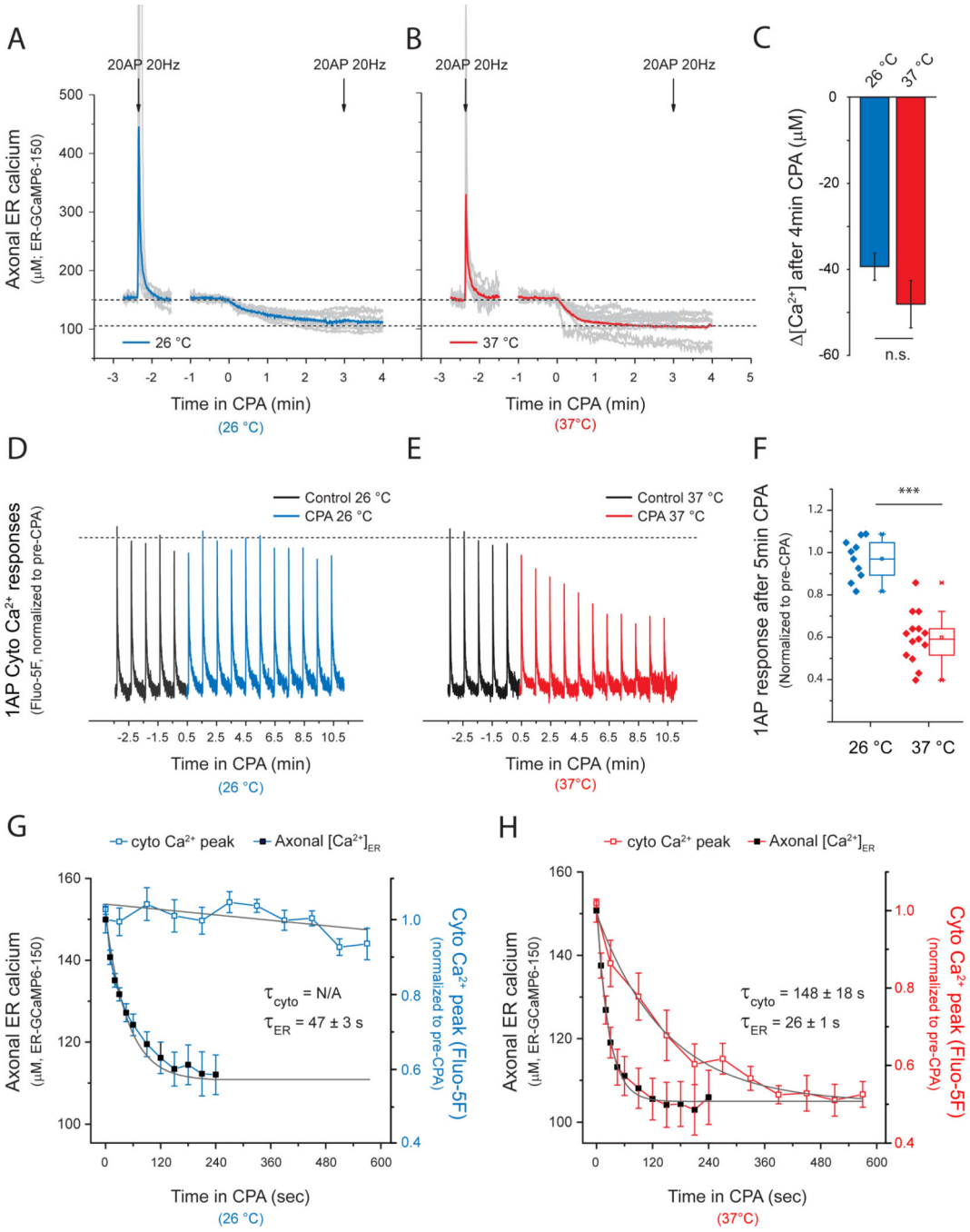

Figure 5. Presynaptic inhibition is slower than ER Ca^{2+} depletion following SERCA block

(A-C) Average axonal ER Ca^{2+} dynamics were measured using ER-GCaMP6-150 at 26°C, (A, blue) or 37°C (B, red). Grey traces are individual experiments, although some individual responses overshot the scale used here and their peaks were not included in the graph. Neurons were stimulated with 20 AP (20 Hz) and then treated with CPA to induce ER Ca^{2+} depletion. After 3 min of CPA treatment the responses to a second stimulus were abolished (indicated by second arrow, 20AP 20Hz). (C) Estimate of $\Delta[Ca^{2+}]_{ER}$ assuming an average resting $[Ca^{2+}]_{ER}$ based on ionomycin responses; n(26°C)=8, n(37°C)=15; n.s. p=0.36. (D)

Single-AP cytosolic Ca^{2+} responses (Fluo-5F AM, normalized to average pre-CPA ΔF response) every 60s measured before (black traces) and after CPA treatment at 26°C (D, G, blue traces) or 37°C (E, H, red traces). (G, H) Comparison of the kinetics of presynaptic inhibition and axonal ER Ca^{2+} depletion. Curves were fit to single exponential decays where possible and time constants (τ) were obtained for comparison. τ_{ER} (26°C)= 47.5 ± 3.4 s, n=8; τ_{ER} (37°C)= 26 ± 0.9 s, n=15; $\tau_{cyto\ Ca^{2+}}$ (37°C)= 148 ± 18 s, n=7.

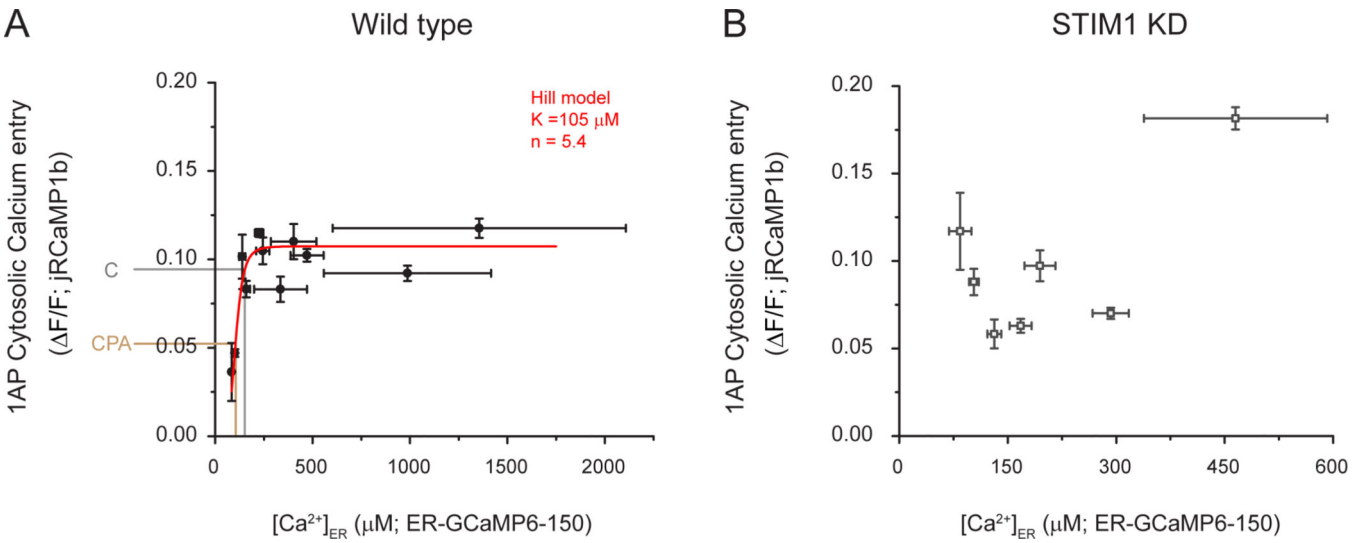

Figure 6. Presynaptic Ca^{2+} influx is correlated with ER Ca^{2+} content in wild type but not in STIM1 KD neurons

(A-B) Neurons expressing ER-GCaMP6-150 and cytosolic jRCaMP1b were co-transfected with or without an shRNA targeting STIM1 and were used to examine single AP-driven Ca^{2+} influx (jRCaMP1b) and axonal $[Ca^{2+}]_{ER}$ (ER-GCaMP6-150) in the same cells. Recordings from wild type (n=15) and STIM1 KD (n=12) neurons were grouped using a binning size of $[Ca^{2+}]_{ER}$=25μM to better estimate fitting parameters (see methods; see Fig. S6 for unbinned data). These two variables are correlated only in wild type cells (A) and are well described by a generalized Hill equation (red line) with a $K_{1/2}$ of 105 μM ± 5 μM and a Hill coefficient of 5.4 ± 2.7(Adjusted R-square = 0.87). Fitting in the case of STIM1 KD was not possible (B, see methods). Grey and brown lines show the predicted impact of CPA on Ca^{2+} influx when the average value of $[Ca^{2+}]_{ER}$ (152 μM) decreases by 48 μM, as measured during SERCA block.

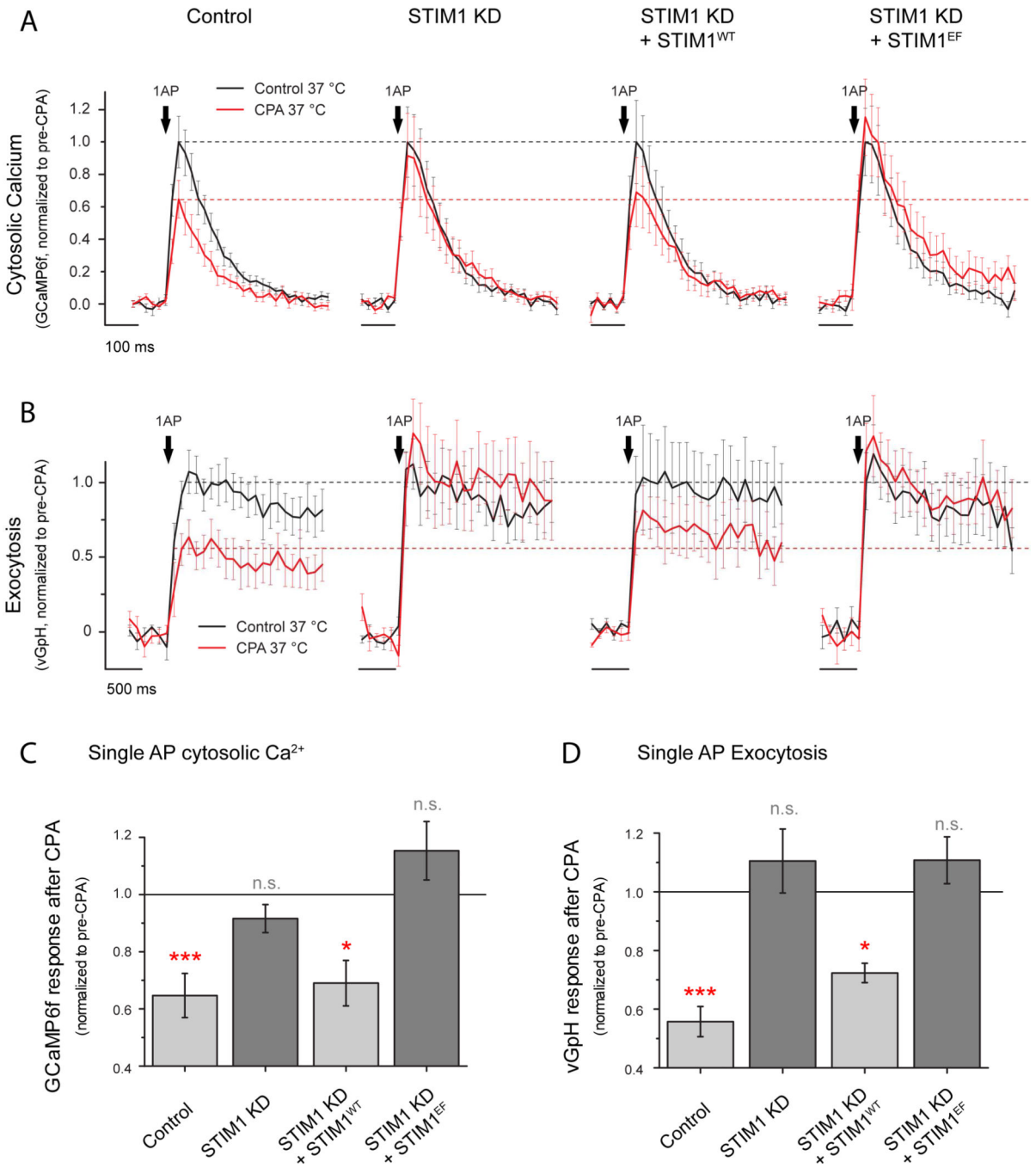

Figure 7. STIM1 regulates presynaptic function impairment induced by ER Ca^{2+} depletion

(A-D) Single AP-driven cytosolic Ca^{2+} signals and exocytosis were measured using GCaMP6f or vG-pH, respectively. Single-AP stimulated signals were quantified in wild type neurons, STIM1 KD neurons, STIM1 KD neurons expressing an shRNA-resistant version of STIM1 ($STIM1^{WT}$) or STIM1 KD neurons expressing an shRNA-resistant version of STIM1 that is insensitive to ER Ca^{2+} content due to EF-hand mutations ($STIM1^{EF}$). Responses were quantified before (black) and after (red) CPA treatment. Black dashed lines represent average response before treatment whereas red dashed lines represent the effect

quantified in wild type neurons for ease of comparison in the different conditions. (C-D) Differential effects of CPA are summarized by showing the remaining response after CPA treatment in each of the conditions. Solid black line indicates response before CPA treatment, normalized to 1 in each case. (C) Effects of CPA in single-AP-driven presynaptic Ca^{2+} signals, Control n=16, ***p=0.0016; STIM1 KD n=14, n.s. p=0.60; STIM1 KD + $STIM1^{WT}$ n=10, *p=0.02; STIM1 KD + $STIM1^{EF}$ n=10, n.s. p=0.14. (D) Effects of CPA in single-AP vG-pH peak responses, Control n=10, ***p=$6.68 \cdot 10^{-5}$; STIM1 KD n=7, n.s. p=0.22; STIM1 KD + $STIM1^{WT}$ n=7, *p=0.031; STIM1 KD + $STIM1^{EF}$ n=7, n.s. p=0.55. Statistics were analyzed using paired sample Student's t-test.

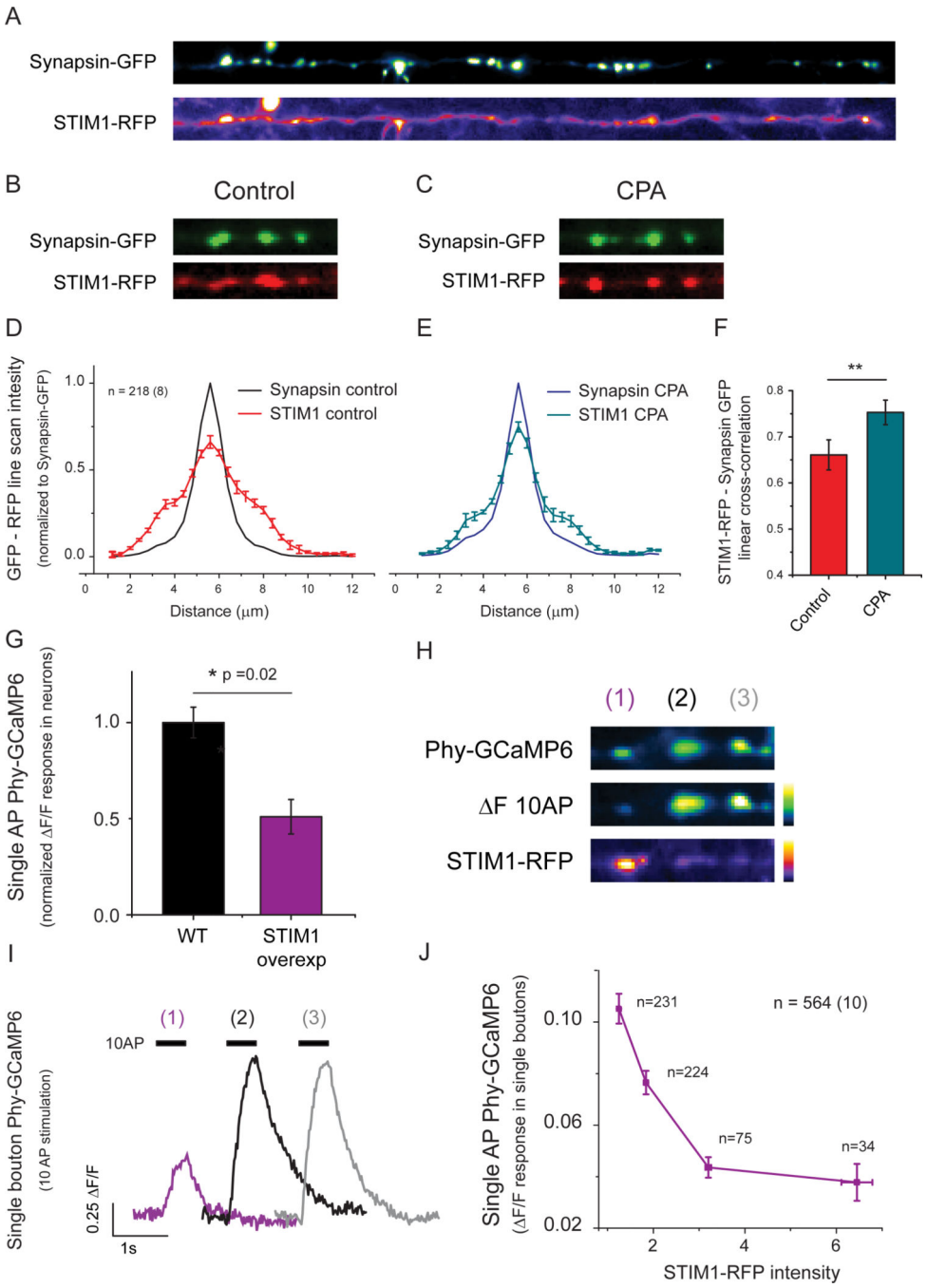

Figure 8. Local STIM1 enrichment at nerve terminals inhibits Ca^{2+} influx

(A) Representative image of an individual axon expressing STIM1-RFP and the presynaptic marker synapsin-GFP (straightened for ease of visualization). (B-E) Synapsin-GFP and STIM1-RFP were imaged before (B) and after CPA treatment (C). (D-F) Intensity profiles of both proteins were analyzed in 218 individual boutons from 8 neurons and compared before and after 15 min of CPA treatment to obtain 1 dimensional intensity cross-correlation profiles, showing that the presynaptic enrichment of STIM1-RFP increases following CPA treatment (F; control=0.66 ± 0.03, CPA=0.75 ± 0.02; ** p=0.0012) with negligible impact

on the distribution of synapsin-GFP (control, black profile in D; CPA, blue profile in E). (G) Average decrease in single AP-Ca^{2+} influx following overexpression of STIM1-RFP. (H) Representative image of a neuron co-transfected with Phy-GCaMP6 (top, left) and STIM1-RFP (bottom left) showing the response to a 10 AP stimulus (middle left). Note that nerve terminals with greater STIM1-RFP abundance (1) have lower Ca^{2+} influx than neighboring synapses (2,3) with lower STIM1-RFP abundance (right) (I) Quantification of 10AP-driven phy-GCaMP6 signals shown in H. (J) Quantification of single AP-driven phy-GCaMP6 signals and their corresponding STIM1-RFP intensities acquired from 564 individual boutons from 10 neurons co-transfected as in H. STIM1-RFP intensities are shown as fluorescence normalized to the auto-fluorescence. Phy-GCaMP6 responses were binned into 4 different STIM1-RFP intensity groups (1–1.5, 1.5–2.5, 2.5–4.5 and >4.5) and reveal a strong inverse correlation between STIM1-RFP abundance and Ca^{2+} influx.

Table 1

Mutations in GCaMP3 to generate low-affinity Ca^{2+} indicators with high sensitivity

Mutations on GCaMP3 are performed in the circularly-permutated EGFP domain (cpEGFP), in the linker region or in the calmodulin domain.

Indicator	cpEGFP	Linker		Calmodulin									
GCaMP3-44							**D362I**						
GCaMP6-150	**K78H**	**T302L**	**R303P**	**A317E**	**D324G**	**D360G**		**D380Y**	**T381R**	**S383T**	**R392G**		
GCaMP6-210	**K78H**	**T302L**	**R303P**	**A317E**	**D324G**	**D360G**		**D380Y**	**T381R**	**S383T**	**R392G**	**D397G**	
GCaMP3-373					**D324G**	**D360G**						**D397G**	**D435G**